4.3 Salt is often added to icy roads in winter. Could DTA be used to quantify the effects of salt on ice? What results would you expect?

References

T. Daniels (1973). *Thermal Analysis*, Kogan Page.
R. C. Mackenzie (1970). *Differential Thermal Analysis*, Vols I and II, Academic Press.
M. I. Pope and M. D. Judd (1977). *Differential Thermal Analysis*, Heyden.
W. W. Wendlandt (1974). *Thermal Methods of Analysis*, Wiley.

Chapter 5

X-ray Diffraction

Undoubtedly the most important and useful technique in solid state chemistry, X-ray diffraction, has been in use since the early part of this century for the fingerprint characterization of crystalline materials and for the determination of their crystal structures. This chapter deals with the basic principles of diffraction and describes in some detail the powder method and its applications. A brief description of single crystal methods and their applications is given. The methods used for solving crystal structures are largely omitted but sections are included that together with Chapter 6 may help guide the reader through the crystallographic literature. It is important to be able to comprehend papers that report new crystal structures without necessarily going into the mathematics of the methods that are used to solve them.

5.1 X-rays and their generation

X-rays are electromagnetic radiation of wavelength ~ 1Å (10^{-10}m). They occur in that part of the electromagnetic spectrum between γ-rays and the

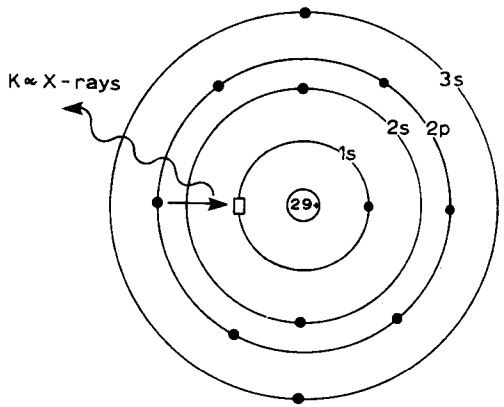

Fig. 5.1 Generation of Cu $K\alpha$ X-rays. A $2p$ electron falls into the empty $1s$ level (□) and the excess energy is released as X-rays

ultraviolet. X-rays are produced when high energy charged particles, e.g. electrons accelerated through 30000 V, collide with matter. The electrons are slowed down or stopped by the collision and some of their lost energy is converted into electromagnetic radiation. Such processes give 'white radiation', X-rays which have wavelengths ranging upwards from a certain lower limiting value. This lower wavelength limit corresponds to the X-rays of highest energy and occurs when all the kinetic energy of the incident particles is converted into X-rays. It may be calculated from the formula, λ_{min}(Å) = 12400/V, where V is the accelerating voltage.

The X-rays which are used in almost all diffraction experiments are produced by a different process that leads to *monochromatic X-rays*. A beam of electrons, again accelerated through, say, 30 kV is allowed to strike a metal *target*, often copper. The incident electrons have sufficient energy to ionize some of the copper $1s$ (K shell) electrons (Fig. 5.1). An electron in an outer orbital ($2p$ or $3p$) immediately drops down to occupy the vacant $1s$ level and the energy released in the transition appears as X-radiation. The transition energies have fixed values and so a spectrum of characteristic X-rays results (Fig. 5.2). For copper, the $2p \rightarrow 1s$ transition, called $K\alpha$, has a wavelength of 1.5418 Å and the $3p \rightarrow 1s$ transition, $K\beta$, 1.3922 Å. The $K\alpha$ transition occurs much more frequently than the $K\beta$ transition and it is this more intense $K\alpha$ radiation which results that is used in diffraction experiments. In fact, the $K\alpha$ transition is a doublet, $K\alpha_1 = 1.54051$ Å and $K\alpha_2 = 1.54433$ Å, because the transition has a slightly different energy for the two possible spin states of the $2p$ electron which makes the transition, relative to the spin of the vacant $1s$ orbital. In some X-ray experiments, diffraction by the $K\alpha_1$ and $K\alpha_2$ radiations is not resolved and a single line or spot is observed instead of a doublet (e.g. in powder diffractometry at low angle). In other experiments, separate diffraction peaks may be observed; if desired, this can be overcome by removing the weaker $K\alpha_2$ beam from the incident radiation (Sections 5.6.1 and 5.6.2).

The wavelengths of the $K\alpha$ lines of the target metals commonly used for X-ray generation are given in Table 5.1. The wavelengths are related to the atomic number, Z, of the metal, by *Moseley's Law*:

$$f^{1/2} = \left(\frac{c}{\lambda}\right)^{1/2} \propto Z \qquad (5.1)$$

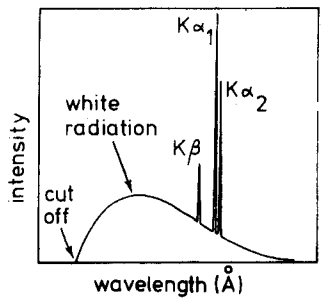

Fig. 5.2 X-ray emission spectrum of a metal, e.g. copper

Table 5.1 *X-ray wavelengths of commonly used target materials*

Target	$K\alpha_1$	$K\alpha_2$	$K\bar{\alpha}$*	Filter
Cr	2.2896	2.2935	2.2909	V
Fe	1.9360	1.9399	1.9373	Mn
Cu	1.5405	1.5443	1.5418	Ni
Mo	0.7093	0.7135	0.7107	Nb
Ag	0.5594	0.5638	0.5608	Pd

* $\bar{\alpha}$ is the intensity-weighted average of α_1 and α_2.

where f is the frequency of the $K\alpha$ line. Hence the wavelength of the $K\alpha$ line decreases with increasing atomic number.

The X-ray emission spectrum of an element such as copper (Fig. 5.2) has two main features. The intense, monochromatic peaks, caused by electronic transitions within the atoms, have wavelengths that are characteristic of the element i.e. copper. These monochromatic peaks are superposed on a background of 'white' radiation, mentioned earlier, which is produced by the general interaction of high velocity electrons with matter. In order to generate the characteristic monochromatic radiation, the voltage used to accelerate the electrons needs to be sufficiently high ($\gtrsim 10\,\text{kV}$) so that ionization of the copper 1*s* electrons may occur.

In the generation of X-rays (Fig. 5.3), the electron beam, provided by a heated tungsten filament, is accelerated towards an anode by a potential difference of $\sim 30\,\text{kV}$. The electrons strike the target, a piece of copper fixed to the anode, and a spectrum of X-rays, such as shown in Fig. 5.2, is emitted. The chamber, known as the *X-ray tube*, is evacuated in order to avoid collisions between air particles and either the incident electrons or emitted X-rays. The X-rays leave the tube through 'windows' made of beryllium. The absorption of X-rays on passing through materials depends on the atomic weight of the elements present in the material. Beryllium with an atomic number of 4 is, therefore, one of the most suitable window materials. For the same reason, lead is a very effective material for shielding X-ray equipment and absorbing stray radiation. While an X-ray tube is in operation, continuous cooling of the anode is necessary. Only a small fraction of the energy of the incident electron beam is converted into X-rays. Most of the

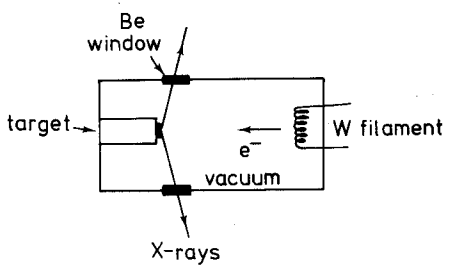

Fig. 5.3 Schematic design of a filament X-ray tube

energy is converted into heat and the anode would soon melt if it were not cooled.

For most diffraction experiments, a monochromatic beam of X-rays is desired and not a continuous spectrum. In the spectrum of X-rays emitted by copper (or any metal), the $K\alpha$ line(s) is the most intense and it is desired to filter out all the other wavelengths, leaving the $K\alpha$ line for diffraction experiments. For copper radiation, a sheet of nickel foil is very effective in carrying out this separation. The energy required to ionize 1*s* electrons of nickel corresponds to a wavelength of 1.488 Å, which lies between the values for the $K\alpha$ and $K\beta$ lines of the copper emission spectrum. Cu $K\beta$ radiation, therefore, has sufficient energy to ionize 1*s* electrons of nickel whereas Cu $K\alpha$ radiation does not. Nickel foil is effective in absorbing the Cu $K\beta$ radiation and most of the white radiation, leaving a monochromatic, reasonably clean beam of $K\alpha$ radiation. A lighter element, such as iron, would absorb $K\alpha$ radiation as well as $K\beta$, because its *absorption edge* is displaced to higher wavelengths. On the other hand, a heavier element, such as zinc, would transmit both $K\alpha$ and $K\beta$ radiations while still absorbing much of the higher energy white radiation. The atomic number of the element in the filter generally is one or two less than that of the target material, (Table 5.1). An alternative method of obtaining monochromatic X-rays uses a single crystal monochromator and is discussed in Section 5.6.2.

5.2 Diffraction

5.2.1 An optical grating and diffraction of light

As an aid to understanding the diffraction of X-rays by crystals, let us consider the diffraction of light by an optical grating. This gives a 1-dimensional analogue of the three-dimensional process that occurs in crystals.

An optical grating may consist of a piece of glass on which have been ruled a large number of accurately parallel and closely spaced lines. The separation of the lines should be a little larger than the wavelength of light, say 10000 Å. The grating is shown in projection as a row of points in Fig. 5.4. Consider what happens to a beam of light which hits the grating perpendicular to the plane of the grating. A piece of glass without the lines would simply transmit the light, but in the grating the lines act as secondary point (or, rather, line) sources of light and re-

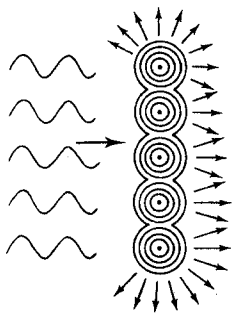

Fig. 5.4 Lines on an optical grating act as secondary sources of light

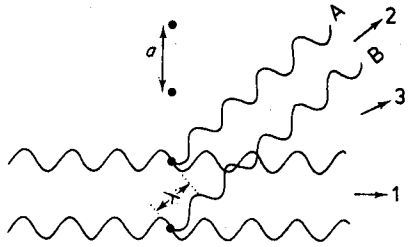

Fig. 5.5 Constructive interference in directions 1 and 2

radiate light in all directions. Interference then occurs between the waves originating from each line source. In certain directions, adjacent beams are in phase with each other and *constructive interference* occurs to give a resultant diffracted beam in that direction. Two such directions are shown in Fig. 5.5. In direction 1, parallel to the incident beam, the diffracted beams are obviously in phase. In direction 2, the beams are also in phase although beam B is now exactly one wavelength behind beam A. At directions between 1 and 2, beam B lags behind beam A by a fraction of one wavelength, and *destructive interference* occurs. For a certain direction, 3, B is exactly half a wavelength behind A and complete destructive interference or *cancellation* occurs. For other directions between 1 and 2, the destructive interference is only partial. Thus, directions 1 and 2 have maximum light intensity and this falls off gradually to zero as the angle changes to direction 3. In the optical grating, however, there are not just two parallel diffracted beams A and B but several hundred or thousand, one for each line on the grating. This causes the resultant diffracted beams to sharpen enormously after interference so that intense beams occur in directions 1 and 2 with virtually no intensity over the whole range of directions between 1 and 2.

The directions, such as 2, in which constructive interference occurs are governed by the wavelength of the light, λ, and the separation, a, of the lines on the grating. Consider the diffracted beams 1 and 2 (Fig. 5.6) which are at an angle, ϕ, to the direction of the incident beam. If 1 and 2 are in phase with each other, the

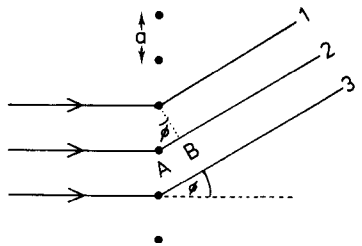

Fig. 5.6 Diffraction of light by an optical grating

distance AB must equal a whole number of wavelengths; i.e.

$$AB = \lambda, 2\lambda, \ldots, n\lambda$$

But

$$AB = a \sin \phi$$

Therefore,

$$a \sin \phi = n\lambda \tag{5.2}$$

This equation gives the conditions under which constructive interference occurs and relates the spacing of the grating to the light wavelength and the diffraction order, n. Hence, depending on the value of $a \sin \phi$, one or more diffraction orders, corresponding to $n = 1, 2$, etc., may be observed.

We can now understand why the separation of the lines on the grating must be of the same order of magnitude as, but somewhat larger than, the wavelength of light. The condition for the first order diffracted beam to occur is $a \sin \phi = \lambda$. The maximum value of $\sin \phi$ is 1, corresponding to $\phi = 90°$ but realistically, in order to observe first order diffraction, $\sin \phi < 1$ and, therefore, $a > \lambda$. If $a < \lambda$, only the zero order direct beam is observable.

If, on the other hand, $a \gg \lambda$, individual diffraction orders ($n = 1, 2, 3, \ldots$, etc.) are so close together as to be unresolved and, effectively, a diffraction continuum results. This is because, for large values of a, $\sin \phi$ and, hence, ϕ must be very small. Therefore $\phi_{n=1} \gtrsim 0$ and the first order beam is not distinguishable from the primary beam. Visible light has wavelengths in the range 4000 to 7000 Å and so, in order to observe well-separated spectra, grating spacings are usually 10000 to 20000 Å.

The other condition to be observed in the construction of an optical grating is that the lines should be accurately parallel. If this were not so, ϕ would vary over the grating and the diffraction spectra would be blurred or irregular and of poor quality generally.

5.2.2 Crystals and diffraction of X-rays

By analogy with the diffraction of light by an optical grating, crystals, with their regularly repeating structures, should be capable of diffracting radiation that has a wavelength similar to the interatomic separation, ~ 1 Å. Three types of radiation are used for crystal diffraction studies: X-rays, electrons and neutrons. Of these, X-rays are by far the most useful but electron and neutron diffraction both have important specific applications and are discussed in Chapter 3.

The X-ray wavelength commonly employed is the characteristic $K\alpha$ radiation, $\lambda = 1.5418$ Å, emitted by copper. When crystals diffract X-rays, it is the atoms or ions which act as secondary point sources and scatter the X-rays; in the optical grating, it is the lines scratched or ruled on the glass surface which cause scattering.

Historically, two approaches have been used to treat diffraction by crystals. These are as follows.

5.2.2.1 *The Laue equations*

Diffraction from a hypothetical 1-dimensional crystal, constituting a row of atoms, may be treated in the same way as diffraction of light by an optical grating because, in projection, the grating is a row of points. An equation is obtained which relates the separation, a, of the atoms in the row, the X-ray wavelength, λ, and the diffraction angle, ϕ; i.e.

$$a \sin \phi = n\lambda$$

A real crystal is a three-dimensional arrangement of atoms for which three *Laue equations* may be written:

$$a_1 \sin \phi_1 = n\lambda$$
$$a_2 \sin \phi_2 = n\lambda$$
$$a_3 \sin \phi_3 = n\lambda$$

Each equation corresponds to the diffraction condition for rows of atoms in one particular direction and three directions or axes are needed in order to represent the atomic arrangement in the crystal. For a diffracted beam to occur, these three equations must all be satisfied simultaneously.

The Laue equations provide a rigorous and mathematically correct way to describe diffraction by crystals. The drawback is that they are cumbersome to use. The alternative theory of diffraction, based on Bragg's Law, is much simpler and is used almost universally in solid state chemistry. No further discussion of the Laue equations is given in this book.

5.2.2.2 *Bragg's Law*

The Bragg approach to diffraction is to regard crystals as built up in layers or planes such that each acts as a semi-transparent mirror. Some of the X-rays are reflected off a plane with the angle of reflection equal to the angle of incidence, but the rest are transmitted to be subsequently reflected by succeeding planes.

The derivation of Bragg's Law is shown in Fig. 5.7. Two X-ray beams, 1 and 2, are reflected from adjacent planes, A and B, within the crystal and we wish to

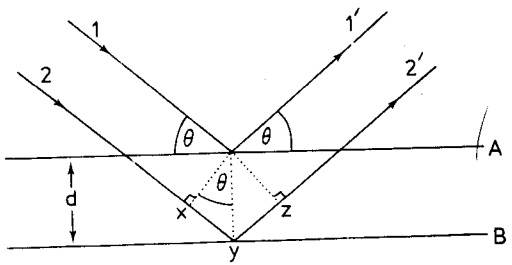

Fig. 5.7 Derivation of Bragg's Law for X-ray diffraction

know under what conditions the reflected beams 1′ and 2′ are in phase. Beam 22′ has to travel the extra distance xyz as compared to beam 11′, and for 1′ and 2′ to be in phase, distance xyz must equal a whole number of wavelengths. The perpendicular distance between pairs of adjacent planes, the *d-spacing*, d, and the angle of incidence, or *Bragg angle*, θ, are related to the distance xy by

$$xy = yz = d \sin \theta$$

Thus

$$xyz = 2d \sin \theta$$

But

$$xyz = n\lambda$$

Therefore

$$2d \sin \theta = n\lambda \qquad \textit{Bragg's Law} \tag{5.3}$$

When Bragg's Law is satisfied, the reflected beams are in phase and interfere constructively. At angles of incidence other than the Bragg angle, reflected beams are out of phase and destructive interference or cancellation occurs. In real crystals, which contain thousands of planes and not just the two shown in Fig. 5.7, Bragg's Law imposes a stringent condition on the angles at which reflection may occur. If the incident angle is incorrect by more than a few tenths of a degree, cancellation of the reflected beams is usually complete.

For a given set of planes, several solutions of Bragg's Law are usually possible, for $n = 1, 2, 3$, etc. It is customary, however, to set n equal to 1 and for situations where, say, $n = 2$, the d-spacing is instead halved by doubling up the number of planes in the set; hence n is kept equal to 1. (Note that $2\lambda = 2d \sin \theta$ is equivalent to $\lambda = 2(d/2) \sin \theta$.)

It is difficult to give an explanation of the nature of the semi-transparent layers or planes that is immediately convincing. This is because they are a concept rather than a physical reality. Crystal structures, with their regularly repeating patterns, may be referred to a three-dimensional grid and the repeating unit of the grid, the *unit cell* (see the next section), can be found. The grid may be divided up into sets of planes in various orientations and it is these planes which are considered in the derivation of Bragg's Law. In some cases, with simple crystal structures, the planes do correspond to layers of atoms, but this is not generally the case.

Some of the assumptions upon which Bragg's Law is based may seem to be rather dubious. For instance, it is known that diffraction occurs as a result of interaction between X-rays and atoms. Further, the atoms do not *reflect* X-rays but scatter or diffract them in all directions. Nevertheless, the highly simplified treatment that is used in deriving Bragg's Law gives exactly the same answers as are obtained by a rigorous mathematical treatment. We therefore happily use terms such as reflexion (often deliberately spelt incorrectly!) and bear in mind that we are fortunate to have such a simple and picturesque, albeit inaccurate, way to describe what in reality is a very complicated process. Further discussion of Bragg's Law and diffraction must wait until we have considered some basic rules and definitions about the symmetry and structures of crystals.

5.3 Definitions

5.3.1 Unit cells and crystal systems

Crystals are built up of a regular arrangement of atoms in three dimensions; this arrangement can be represented by a repeat unit or motif called the *unit cell.* The unit cell is defined as *the smallest repeating unit which shows the full symmetry of the crystal structure.* Let us see exactly what this means, first of all in two dimensions. A section through the NaCl structure is shown in Fig. 5.8(a). Possible repeating units are given in Fig. 5.8(b) to (e). In each, the repeat unit is a square and adjacent squares share edges and corners. Adjacent squares are identical, as they must be by definition; thus, all the squares in (b) have Cl^- ions at their corners and centres. The repeat units in (b), (c) and (d) are all of the same size and, in fact, differ only in their relative position. This brings us to an important point. The choice of origin of the repeating unit is to a certain extent a matter of personal taste, even though the size and shape or orientation of the cell are fixed. The repeat unit of NaCl is usually chosen as either (b) or (c) rather than (d) because it is easier to draw the unit and visualize the structure as a whole if the unit contains atoms or ions at special positions such as corners, edge centres, etc. Another guideline is that the origin is usually chosen so that the symmetry of the structure is evident (Section 5.3.3).

In the hypothetical case that two-dimensional crystals of NaCl could be formed, the repeat unit shown in Fig. 5.8(e) or its equivalent, with chlorine at the corners and sodium in the middle, would be the correct unit. Comparing (e) and, for example, (b), both are square and show the symmetry of the structure; as (e) is half the size of (b), (e) would be preferred according to the definition of the unit cell

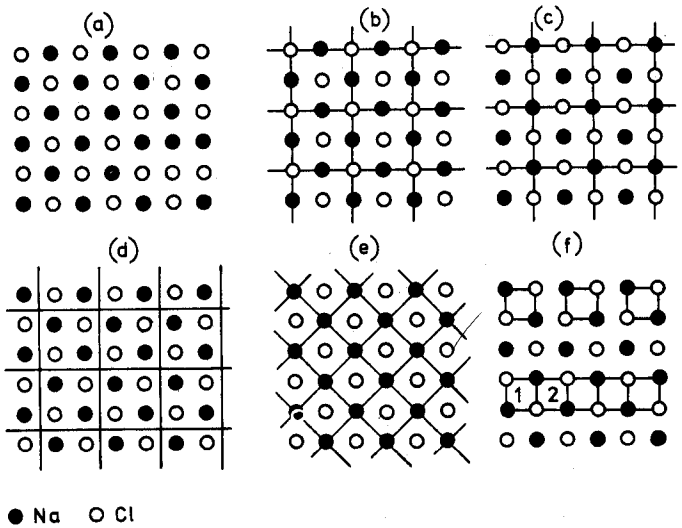

Fig. 5.8 (a) Section through the NaCl structure, showing (b) to (e) possible repeat units and (f) incorrect units

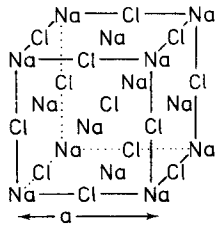

Fig. 5.9 Cubic unit cell of NaCl, $a = b = c$

given above. In three dimensions, however, the unit cell of NaCl is based on (b) rather than (e) because only (b) shows the cubic symmetry of the structure (Section 5.3.3).

In Fig. 5.8(f) are shown two examples of what is *not* a repeat unit. The top part of the diagram contains isolated squares whose area is one quarter of the squares in (b). It is true that each square is identical but it is not permissible to isolate unit cells or areas from each other, as appears to happen here. The bottom part of the diagram contains units that are not identical; thus square 1 has a sodium in its top right corner whereas 2 has a chlorine in this position.

The unit cell of NaCl in three dimensions in shown in Fig. 5.9; it contains Na^+ ions at the corners and face centre positions with Cl^- ions at the edge centres and body centre. Each face of the unit cell looks like the unit area shown in Fig. 5.8(c). As in the two-dimensional case, the choice of origin is somewhat arbitrary and an equally valid unit cell could be chosen in which the Na^+ and Cl^- ions were interchanged. The unit cell of NaCl is cubic. The three edges of the cell, a, b and c are equal in length. The three angles of the cell α (between b and c), β (between a and c) and γ (between a and b) are all equal to 90°. A cubic unit cell also possesses certain symmetry elements, and these symmetry elements together with the shape define the cubic unit cell.

The seven *crystal systems* listed in Table 5.2 are the seven independent unit cell shapes that are possible in three-dimensional crystal structures. Each crystal system is governed by the presence or absence of symmetry in the structure and the essential symmetry for each is given in the third column. Let us next deal with symmetry because it is of fundamental importance in solid state chemistry and, especially, in crystallography.

5.3.2 Symmetry, point symmetry and point groups

Symmetry is most easily defined by the use of examples. Consider the silicate tetrahedron shown in Fig. 5.10(a). If it is rotated about an axis passing along one of the Si—O bonds, say the vertical one, then every 120° the tetrahedron finds itself in an identical position. Effectively, the three basal oxygens change position with each other every 120°. During a complete 360° rotation, the tetrahedron passes through three such identical positions. The fact that different (i.e. > 1) identical orientations are possible means that the SiO_4 tetrahedron possesses symmetry. The axis about which the tetrahedron may be rotated is called a *symmetry element* and the process of rotation a *symmetry operation.*

Table 5.2 *The seven crystal systems*

Crystal system	Unit cell shape†	Essential symmetry	Space lattices
Cubic	$a = b = c,\ \alpha = \beta = \gamma = 90°$	Four threefold axes	P, F, I
Tetragonal	$a = b \neq c,\ \alpha = \beta = \gamma = 90°$	One fourfold axis	P, I
Orthorhombic	$a \neq b \neq c,\ \alpha = \beta = \gamma = 90°$	Three twofold axes or mirror planes	P, F, I, A(B or C)
Hexagonal	$a = b \neq c,\ \alpha = \beta = 90°, \gamma = 120°$	One sixfold axis	P
Trigonal (a)	$a = b \neq c,\ \alpha = \beta = 90°, \gamma = 120°$	One threefold axis	P
(b)	$a = b = c,\ \alpha = \beta = \gamma \neq 90°$	One threefold axis	R
Monoclinic*	$a \neq b \neq c,\ \alpha = \gamma = 90°, \beta \neq 90°$	One twofold axis or mirror plane	P, C
Triclinic	$a \neq b \neq c,\ \alpha \neq \beta \neq \gamma \neq 90°$	None	P

*Two settings of the monoclinic cell are used in the literature. The one given here, which is most commonly used, and the other $a \neq b \neq c, \alpha = \beta = 90°, \gamma \neq 90°$.
†The symbol ≠ means not necessarily equal to. Sometimes, crystals possess *pseudo-symmetry* in which, say, the unit cell is geometrically cubic but does not possess the essential symmetry elements for cubic symmetry, and the symmetry is lower, perhaps tetragonal.

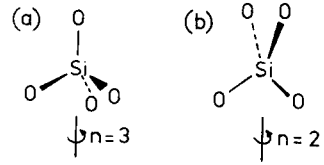

Fig. 5.10 (a) Threefold and (b) twofold rotation axes

The symmetry elements that are important in crystallography are listed in Table 5.3. There are two nomenclatures for labelling symmetry elements, the Hermann–Mauguin system used in crystallography and the Schönflies system used in spectroscopy. It would be ideal if there was only one system which everybody used, but this is unlikely to come about since (a) both systems are very well established and (b) crystallographers require elements of space symmetry that spectroscopists do not, and vice versa, (c) spectroscopists use a more extensive range of point symmetry elements than crystallographers.

The symmetry element described above for the silicate tetrahedron is a *rotation axis*, with symbol n. Rotation about this axis by $360/n$ degrees gives an identical orientation and the operation is repeated n times before the original configuration is regained. In this case, $n = 3$ and the axis is a *threefold rotation axis.* The SiO_4 tetrahedron possesses four threefold rotation axes, one in the direction of each Si—O bond.

When viewed from another angle, SiO_4 tetrahedra possess twofold rotation axes (Fig. 5.10b) which pass through the central silicon and bisect the O—Si—O bonds. Rotation by 180° leads to an indistinguishable orientation of the tetrahedron. The tetrahedron possesses three of these twofold axes. (According to the Schönflies system, there are six twofold axes; each axis is counted twice, to include the two possible directions of each axis, i.e. up or down). The *identity operation* corresponds to $n = 1$ (rotation by 360°). It is apparently trivial, being equivalent to doing nothing, but it is important in the application of group theory to point symmetry.

Table 5.3 *Symmetry elements*

	Symmetry element	Notation: Hermann–Mauguin (crystallography)	Notation: Schönflies (spectroscopy)
Point symmetry	Mirror plane	m	σ_v, σ_h
	Rotation axis	$n(= 2, 3, 4, 6)$	$C_n(C_2, C_3, \text{etc.})$
	Inversion axis	$\bar{n}(= \bar{1}, \bar{2}, \text{etc.})$	—
	Alternating axis (rotoreflection)	—	$S_n(S_1, S_2, \text{etc.})$
	Centre of symmetry	$\bar{1}$	i
Space symmetry	Glide plane	n, d, a, b, c	—
	Screw axis	$2_1, 3_1, \text{etc.}$	—

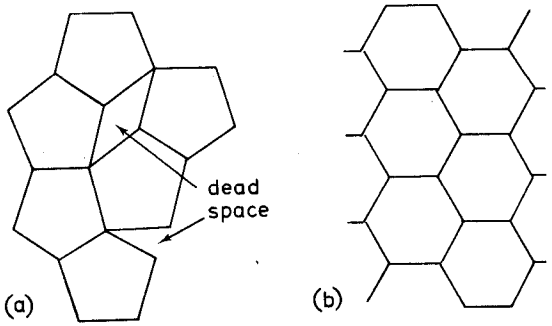

Fig. 5.11 (a) The impossibility of forming a close packed array of pentagons. (b) A close packed layer of hexagons.

Crystals may display rotational symmetries of 1, 2, 3, 4 and 6. Others, such as $n = 5, 7$, are never observed. This is not to say that molecules which have pentagonal symmetry cannot exist in the crystalline state. They can, of course, but their fivefold symmetry cannot be exhibited by the crystal as a whole. This is shown in Fig. 5.11(a), where a fruitless attempt has been made to pack together pentagons to form a complete layer; for hexagons with sixfold rotation axes (b) a close packed layer is easily produced.

A *mirror plane*, *m*, exists when two halves of a molecule or ion can be interconverted by carrying out the imaginary process of reflection across the mirror plane. The silicate tetrahedron possesses three mirror planes, one of which is shown in Fig. 5.12(a). The silicon and two oxygens lie on the mirror plane and are unaffected by the process of reflection. The other two oxygens are interchanged on reflection.

The *centre of symmetry*, $\bar{1}$, exists when any part of a molecule or ion can be reflected through this centre of symmetry, which is a point, and an identical arrangement found on the other side. An $Si_2O_7^{6-}$ group which has a linear Si–O–

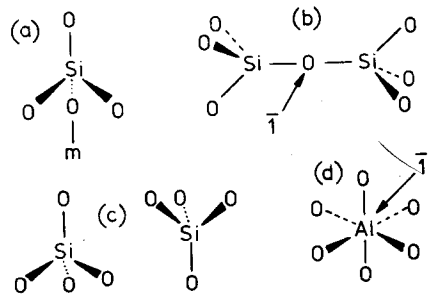

Fig. 5.12 Symmetry elements: (a) mirror plane, (b) centre of symmetry, (c) absence of centre of symmetry in a tetrahedron, (d) centre of symmetry in an octahedron

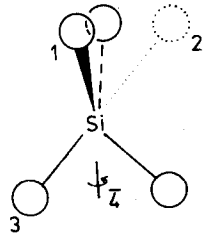

Fig. 5.13 Fourfold inversion axis

Si bridge (it is not usually linear) and with the two SiO_4 tetrahedra in the staggered conformation has a centre of symmetry at the bridging oxygen (Fig. 5.12b). If a line is drawn from any oxygen, through the centre of symmetry and extended an equal distance on the other side, it terminates at another oxygen. A single tetrahedron (e.g. SiO_4) does not have a centre of symmetry (located at Si); the two orientations of the tetrahedra in Fig. 5.12(c) are not identical. On the other hand an octahedron, e.g. AlO_6, is centrosymmetric (Fig. 5.12d).

The *inversion axis*, $\bar{n}$, is a combined symmetry operation involving rotation (according to n) and inversion through the centre. A $\bar{4}$ (fourfold inversion) axis is shown in Fig. 5.13. The first stage involves rotation by $360/4 = 90°$ and takes, for example, oxygen 1 to position 2. This is followed by inversion through the centre, at Si, and leads to the position of oxygen 3. Oxygens 1 and 3 are therefore related by a $\bar{4}$ axis. Possible inversion axes in crystals are limited to $\bar{1}, \bar{2}, \bar{3}, \bar{4}$ and $\bar{6}$ for the same reason that only certain pure rotation axes are allowed. The onefold inversion axis is simply equivalent to the centre of symmetry and the twofold inversion axis is the same as a mirror plane perpendicular to that axis.

The symmetry elements discussed so far are elements of *point symmetry*. For all of them, at least one point stays unchanged during the symmetry operation, i.e. an atom lying on a centre of symmetry, a rotation axis or a mirror plane does not move during the respective symmetry operations. Finite-sized molecules can only possess point symmetry elements, whereas crystals may have extra symmetries that include translation steps as part of the symmetry operation. Many molecules and crystals possess more than one element of point symmetry, but the number of combinations of symmetry elements that may occur in crystals is limited to 32. These are known as the crystallographic *point groups*.

5.3.3 Symmetry: the choice of unit cell and crystal system

The geometric shapes of the various crystal systems (unit cells) are listed in Table 5.2. These shapes do not *define* the unit cell; they are merely a consequence of the presence of certain symmetry elements. A cubic unit cell is defined as one having four three-fold symmetry axes (Fig. 5.14) and it is an automatic consequence of this condition that $a = b = c$ and $\alpha = \beta = \gamma = 90°$. The *essential* symmetry elements by which each crystal system is defined are listed in Table 5.2. In most crystal systems, other symmetry elements are also present. For instance, cubic crystals have many others, including three four-fold axes passing through the centres of each pair of opposite cube faces (Fig. 5.14).

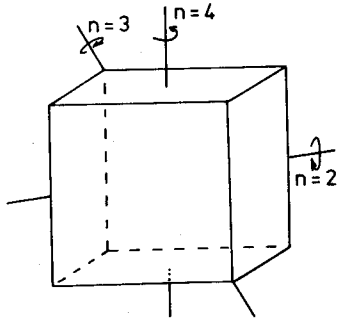

Fig. 5.14 Two-, three- and four-fold axes of a cube

The *tetragonal* unit cell is characterized by a single fourfold axis and is exemplified by the structure of CaC_2. This is related to the NaCl structure but, because the carbide ion is cigar-shaped rather than spherical, one of the cell axes becomes longer than the other two (Fig. 5.15a). A similar tetragonal cell may be drawn for NaCl by replacing Na for Ca and Cl for C_2; it occupies half the volume of the true, cubic unit cell (Fig. 5.15b). The choice of a tetragonal unit cell for NaCl is rejected because it does not show the full cubic symmetry of the crystal (see Fig. 5.8e and the discussion with it).

The *trigonal* system is characterized by a single threefold axis. Its shape can be derived from that of a cube by stretching or compressing the cube along one of its body diagonals (Fig. 5.16). The threefold axis parallel to this body diagonal is retained but those along the other body diagonal directions are all destroyed. All three cell edges remain the same length and all three angles stay the same but are not equal to 90°. It is possible to describe such a trigonal cell for NaCl with $\alpha = \beta = \gamma = 60°$ where Na^+ ions are at the corners and a Cl^- ion is in the body centre, but this is again unacceptable because NaCl has symmetry higher than trigonal. $NaNO_3$ has a structure that may be regarded as a trigonal distortion of the NaCl structure: instead of spherical Cl^- ions, it has triangular nitrate groups, and the presence of these effectively causes a compression along one body diagonal (or

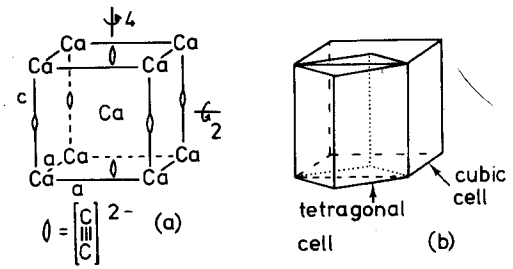

Fig. 5.15 (a) Tetragonal unit cell of CaC_2; (b) relation between tetragonal and cubic cells for NaCl

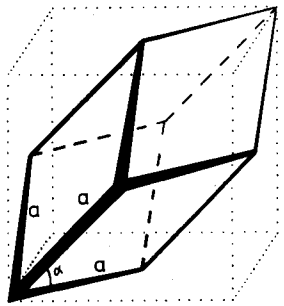

Fig. 5.16 Derivation of a trigonal unit cell from a cubic cell

rather an expansion in the plane perpendicular to the diagonal). All fourfold symmetry axes and all but one of the threefold axes are destroyed.

The trigonal crystal system is one of the most difficult to work with. The trigonal cell can be defined with either rhombohedral axes (as above) or with hexagonal axes (Table 5.2). There has been a controversy among crystallographers lasting for many years over the exact status of the trigonal crystal system. Some claim that it should not be regarded as a separate system but should be included as a subsystem of the hexagonal system. The majority accord it with independent status, however, and it has been treated as such in Table 5.2.

The *hexagonal* crystal system is discussed in some detail in Chapter 7, where a drawing of the hexagonal unit cell is given in Fig. 7.6.

The *orthorhombic* unit cell may be regarded as something like a shoebox in which the angles are all 90° but the sides are of unequal length. It usually possesses several mirror planes of symmetry and several twofold axes; the minimum requirement for orthorhombic symmetry is the presence of three mutually perpendicular mirror planes or twofold axes.

The *monoclinic* unit cell may be regarded as derived from our orthorhombic shoebox by a shearing action in which the top face is partially sheared relative to the bottom face and in a direction parallel to one of the box edges. As a consequence, one of the angles departs from 90° and most of the symmetry is lost, apart from a mirror plane and/or a single twofold axis.

The *triclinic* system possesses no symmetry at all, which is reflected in the shape of the unit cell.

5.3.4 Space symmetry and space groups

The symmetry of finite-sized molecules is limited to the elements of point symmetry whereas crystals, with their infinite repeating structures (for all practical purposes), may also possess elements of *space symmetry*. This involves a combination of point symmetry elements—rotation or mirror plane reflection—with incremental translational steps through the structure.

The *screw axis* combines translation and rotation; the atoms or ions in a crystal which possesses screw axes appear to lie on spirals about these axes. A schematic example is shown in Fig. 5.17(a). The symbol for a screw axis, X_Y,

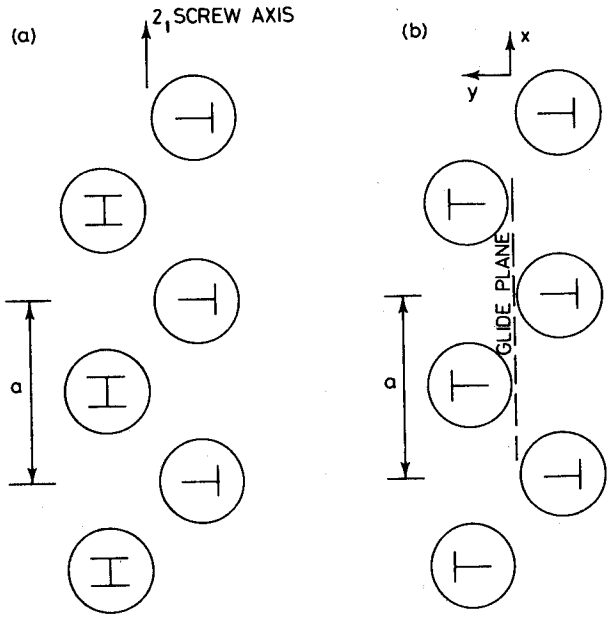

Fig. 5.17 Arrangements of coins with heads (H) and tails (T), illustrating (a) a 2_1 screw axis parallel to *a* and (b) an *a* glide plane perpendicular to *b*

indicates a translation by the fraction Y/X of the unit cell edge in the direction of the screw axis, together with a simultaneous rotation by $\frac{1}{X} \times 360°$ about the screw axis. Thus, a 4_2 axis parallel to *a* involves translation by *a*/2 and rotation by 90°, and this process is repeated twice for every unit cell.

The *glide plane* combines translation and reflection and is shown schematically in Fig. 5.17(b). Translation may be parallel to any of the unit cell axes (*a*, *b*, *c*), to a face diagonal (*n*) or to a body diagonal (*d*). The *a*, *b*, *c* and *n* glide planes all have a translation step of half the unit cell in that direction; by definition, the *d* glide has a translation which is a quarter that of the body diagonal. For the axial glide planes *a*, *b* and *c*, it is important to know both the direction of translation and the reflection plane, e.g. an *a* glide may be perpendicular to *b* (i.e. in the *ac* plane) or perpendicular to *c*.

A fundamental characteristic of crystals and their structures is the *space group*. This is a set of symbols which summarizes information about the crystal system, lattice type and elements of point and space symmetry. Combination of the fourteen Bravais lattices with possible point and space symmetry elements gives rise to a total of 230 possible space groups. Chapter 6 is devoted to space groups and the relation between space groups and crystal structure.

5.3.5 Lattice, Bravais lattice

It is very useful to be able to represent the manner of repetition of atoms, ions or molecules in a crystal by an array of points, the array being called a *lattice* and

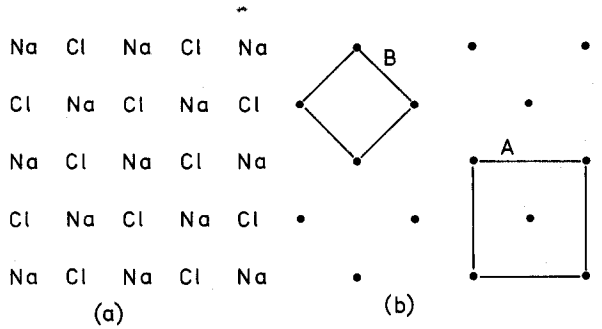

Fig. 5.18 (a) Representation of the NaCl structure in two dimensions by (b) an array of lattice points

the points *lattice points*. The section of the NaCl structure (Fig. 5.18a) may be represented by an array of points (b); each point represents one Na^+ and one Cl^- but whether the point is located at Na^+, at Cl^- or in between is irrelevant. The unit cell may be constructed by linking up the lattice points; two ways of doing this, A and B, are shown in (b). A cell such as B which contains lattice points only at the corners is *Primitive*, P, whereas a cell such as A which contains additional lattice points is *centred*. Several types of centred lattice are possible. The *face centred lattice*, F, contains additional lattice points in the centre of each face (Fig. 5.19a); NaCl is face centred cubic. A *side centred lattice* contains extra lattice points on only one pair of opposite faces, e.g. C-centred (Fig. 5.19b), whereas a *body centred lattice*, I, has an extra lattice point at the body centre (Fig. 5.19c). α-iron is *body centred cubic* because it has a cubic unit cell with iron atoms at the corner and body centre positions. CsCl is also cubic with cesium atoms at corners and chlorine atoms at the body centre (or vice versa), but it is primitive. This is because, in order for a lattice to be body centred, the atom or group of atoms which are located at or near the corner must be identical to those at or near the body centre position.

The combination of crystal system and lattice type gives the *Bravais lattice* of a structure. There are fourteen possible Bravais lattices. They can be deduced from Table 5.2 by taking the different allowed combinations of crystal system and space lattice, e.g. primitive monoclinic, C-centred monoclinic and primitive triclinic are three of the fourteen possible Bravais lattices. The lattice type plus

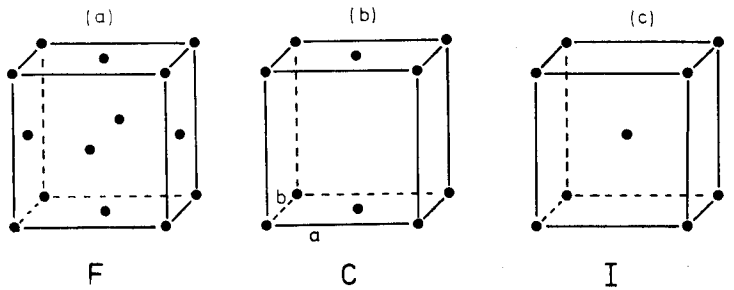

Fig. 5.19 (a) Face centred, (b) side centred and (c) body centred lattices

unit cell combinations which are absent from the table either (a) would violate symmetry requirements, e.g. a C-centred lattice cannot be cubic because it would not have the necessary threefold axes, or (b) may be represented by a smaller, alternative cell, e.g. a face centred tetragonal cell can be redrawn as a body centred tetragonal cell; the symmetry is still tetragonal but the volume is halved (Fig. 5.15b).

5.3.6 Lattice planes, Miller indices and directions

The concept of lattice planes (Section 5.2.2.2) is apparently straightforward but is a source of considerable confusion because there are two separate ideas which can easily become mixed. Any close packed structure, such as metal structures, ionic structures—NaCl, CaF_2, etc.—may, in certain orientations, be regarded as being built up of layers or planes of atoms stacked to form a three-dimensional structure. These layers are often related in a simple manner to the unit cell of the crystal such that, for example, a unit cell face may coincide with a layer of atoms. The reverse is not necessarily true, however, especially in more complex structures, and, for example, unit cell faces or simple sections through the unit cell often do not coincide with layers of atoms in the crystal. *Lattice planes*, which are a concept introduced with Bragg's Law, are defined purely from the shape and dimensions of the unit cell. Lattice planes are entirely imaginary and simply provide a reference grid to which the atoms in the crystal structure may be referred. Sometimes, a given set of lattice planes coincides with layers of atoms, but not usually.

Consider the two-dimensional array of lattice points shown in Fig. 5.20. This array of points may be divided up into many different sets of rows and for each set there is a characteristic perpendicular distance, d, between pairs of adjacent rows. In three dimensions, these rows become planes and adjacent planes are separated by the *interplanar d-spacing*, d. Bragg's Law treats X-ray as being diffracted from these various sets of lattice planes and the Bragg diffraction angle, θ, for each set is related to the d-spacing by Bragg's Law (Section 5.2.2.2).

Lattice planes are labelled by assigning three numbers known as *Miller indices* to each set. The derivation of Miller indices is illustrated in Fig. 5.21. The origin of the unit cell is at point O and two planes are shown which are parallel

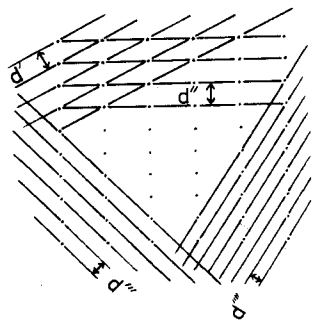

Fig. 5.20 Lattice planes (in projection)

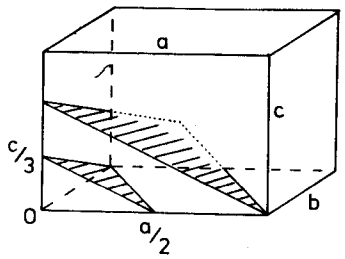

Fig. 5.21 Derivation of Miller indices

and pass obliquely through the unit cell. A third plane in this set must, by definition, pass through the origin. Each of these planes continues out to the surface of the crystal and in so doing cuts through many more unit cells; also, there are many more planes in this set parallel to the two shown, but which do not pass through this particular unit cell. In order to assign Miller indices to a set of planes, first consider that plane which is adjacent to the one that passes through the origin. Second, find the intersection of this plane on the three axes of the cell and write these intersections as fractions of the cell edges. The plane in question cuts the x axis at $a/2$, the y axis at b and the z axis at $c/3$; the fractional intersections are $\frac{1}{2}$, 1, $\frac{1}{3}$. Third, take reciprocals of these fractions; this gives (213). These three integers are the Miller indices of the plane and all other planes that

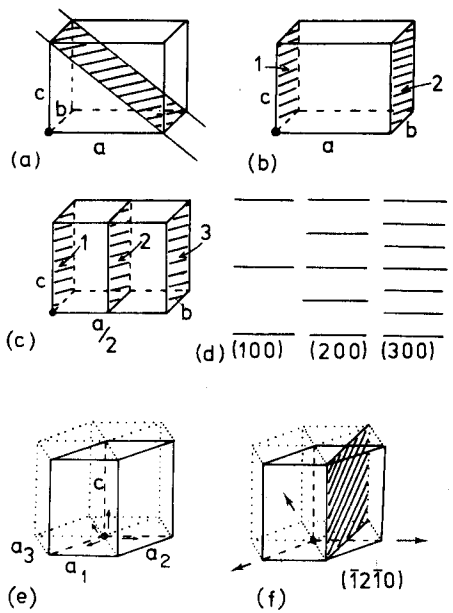

Fig. 5.22 Examples of Miller indices: (a) (101), (b) (100), (c) (200), (d) (h00), (e) labelling of axes in a hexagonal cell, (f) $(\bar{1}2\bar{1}0)$ plane, origin at solid circle, positive a directions indicated by arrows

are parallel to it and are separated from adjacent planes by the same *d*-spacing.

Some other examples are shown in Fig. 5.22. In (a), the shaded plane cuts *x*, *y* and *z* at 1*a*, ∞*b* and 1*c*, i.e. the plane is parallel to *b*. Taking reciprocals of 1, ∞ and 1 gives us (101) for the Miller indices. A Miller index of 0 means, therefore, that the plane is parallel to that axis. In Fig. 5.22(b), the planes of interest comprise opposite faces of the unit cell. We cannot directly determine the indices of plane (1) as it passes through the origin. Plane (2) has intercepts of 1*a*, ∞*b* and ∞*c* and Miller indices of (100). Figure 5.22(c) is similar to (b) but there are now twice as many planes as in (b). To find the Miller indices, consider plane (2) which is the one that is closest to the origin but without passing through it. Its intercepts are $\frac{1}{2}$, ∞ and ∞ and the Miller indices are (200). A Miller index of 2 therefore indicates that the plane cuts the relevant axis at half the cell edge. This illustrates an important point. After taking reciprocals, do not divide through by the highest common factor. A common source of error is to regard, say, the (200) set of planes as those planes interleaved between the (100) planes, to give the sequence (100), (200), (100), (200), (100),.... The correct labelling is shown in Fig. 5.22(d). If extra planes are interleaved between adjacent (100) planes then *all* planes are labelled as (200).

The general symbol for Miller indices is (*hkl*). It is not necessary to use commas to separate the three letters or numbers and the indices are enclosed in curved brackets. The symbol { } is used to indicate sets of planes that are equivalent; for example, the sets (100), (010) and (001) are equivalent in cubic crystals and may be represented collectively as {100}.

Miller indices of planes in hexagonal crystals are an exception in that four indices are often used (*hkil*). The value of the *i* index is derived from the reciprocal of the fractional intercept of the plane in question on the a_3 axis (Fig. 5.22e) in exactly the same way that the other indices are derived. The *i* index is, to a certain extent, a piece of redundant information because the relation $h + k + i = 0$ always holds, as in, for example, $(10\bar{1}1)$, $(\bar{2}110)$, $(1\bar{2}11)$, etc. A bar over an index means that the opposite or negative direction of the corresponding axis was used in defining the indices (see Section 5.3.10). In Fig. 5.22 (f), the $(\bar{1}2\bar{1}0)$ plane is shown as an example. Sometimes hexagonal indices are written with the third index as a dot, e.g. $(\bar{1}2.0)$, and in other cases the *i* index is omitted completely, as in $(\bar{1}20)$.

Directions in crystals and lattices are labelled by first drawing a line that passes

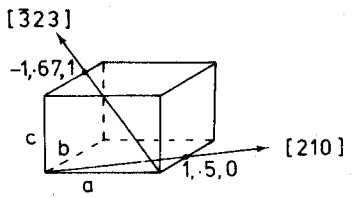

Fig. 5.23 Indices of directions [210] and [3̄23]

through the origin and parallel to the direction in question. Let the line pass through a point with general fractional coordinates *x*, *y*, *z*; the line also passes through 2*x*, 2*y*, 2*z*; 3*x*, 3*y*, 3*z*, etc. These coordinates, written in square brackets [*x*, *y*, *z*], are the indices of the direction; *x*, *y* and *z* are arranged to be the set of smallest possible integers, by division or multiplication throughout by a common factor. Thus $[\frac{1}{2}\frac{1}{2}0]$, [110], [330] all describe the same direction, but conventionally [110] is used. For cubic systems, an [*hkl*] direction is always perpendicular to the (*hkl*) plane of the same indices, but this is only sometimes true in non-cubic systems. Sets of directions which, by symmetry, are equivalent, e.g. cubic [100], [010], etc., are written with the general symbol ⟨100⟩. Some examples of directions and their indices are shown in Fig. 5.23.

5.3.7 *d*-spacing formulae

We have already defined the *d*-spacing of a set of planes as the perpendicular distance between any pair of adjacent planes in the set and it is this *d* value that appears in Bragg's Law. For a cubic unit cell, the (100) planes simply have a *d*-spacing of *a*, the value of the cell edge (Fig. 5.22b). For (200) in a cubic cell, $d = a/2$, etc. For orthogonal crystals (i.e. $\alpha = \beta = \gamma = 90°$), the *d*-spacing for any set of planes is given by the formula

$$\frac{1}{d_{hkl}^2} = \frac{h^2}{a^2} + \frac{k^2}{b^2} + \frac{l^2}{c^2} \tag{5.4}$$

The equation simplifies for tetragonal crystals, in which $a = b$, and still further for cubic crystals with $a = b = c$; i.e. for cubic crystals,

$$\frac{1}{d^2} = \frac{h^2 + k^2 + l^2}{a^2} \tag{5.5}$$

As a check, for cubic (200), $h = 2$, $k = l = 0$ and $1/d^2 = 4/a^2$. Therefore,

$$d = \frac{a}{2}$$

Monoclinic and especially, triclinic crystals have much more complicated *d*-spacing formulae because each angle that is not equal to 90° becomes an additional variable. The relevant formulae for *d*-spacings and unit cell volumes are given in Appendix 6.

5.3.8 Lattice planes and *d*-spacings—how many are possible?

The number of possible sets of lattice planes and their corresponding *d*-spacings is usually large, but finite for two reasons. First, the wavelength of the X-ray beam that is used places a lower limit on the *d*-spacings that may be experimentally observed: from Bragg's Law, $n\lambda = 2d \sin\theta$ and $d = n\lambda/2 \sin\theta$. The maximum value of $\sin\theta$ is 1 (when $2\theta = 180°$) and this places a lower limit on the observed *d*-spacings of $d = \lambda/2$ (for $n = 1$). For Cu $K\alpha$, $\lambda/2 \simeq 0.77$ Å and, if it is

Table 5.4 *Calculated d-spacings for an orthorhombic cell, for* $a = 3.0$, $b = 4.0$, $c = 5.0$ Å

hkl	*d*(Å)
001	5.00
010	4.00
011	3.12
100	3.00
101	2.57
110	2.40
111	2.16

desired to measure *d*-spacings that are smaller than this, the target metal in the X-ray tube must be changed for one which gives a shorter wavelength radiation, e.g. molybdenum (see Table 5.1).

Second, the number of sets of planes is limited because the Miller indices, used in calculating *d*-spacing values can have only integral values (i.e. $h, k, l = 0, 1, 2, \ldots$). There is an inverse relation between *d*-spacing and the magnitude of the Miller indices. Thus, the largest *d*-spacings which may be observed correspond to Miller indices such as (100), (010), (001), (110), etc. If the unit cell dimensions are known, it is possible to calculate all the possible *d*-spacings by substituting values of h, k and l into the appropriate *d*-spacing formula. For example, consider an orthorhombic substance that has cell parameters $a = 3.0$, $b = 4.0$, $c = 5.0$ Å. The *d*-spacings are given by equation (5.4):

$$\frac{1}{d_{hkl}^2} = \frac{h^2}{9} + \frac{k^2}{16} + \frac{l^2}{25}$$

Limiting ourselves to h, k and l values of 0 and 1, the various possible *hkl* combinations and their calculated *d*-spacings are given in Table 5.4. The *hkl* values are listed in order of decreasing *d*-spacing; hence 011 appears above 100. Obviously, the list could be extended for larger h, k, l values and, for example, could be terminated when a certain minimum *d*-spacing had been reached. If h, k, l values of 2 were included then, for example, 002 would appear in the list with a *d*-spacing of 2.5 Å.

5.3.9 Systematically absent reflections

In Section 5.3.8, the factors that govern the *maximum* number of possible lattice planes and *d*-spacings are discussed. In principle, each of these sets of planes will diffract (or reflect) X-rays, but in many cases the resultant intensity is zero. These *absent reflections* may be divided into two groups: those that are absent due to some quirk in the structure and those that are absent due to the symmetry or type of lattice possessed by the structure. The latter are known as *systematic absences*. Systematic absences arise if either the lattice type is non-primitive (I, F, etc.) or if elements of space symmetry (screw axes, glide planes) are present.

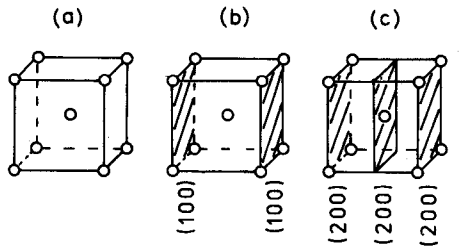

Fig. 5.24 (a) Body centred cubic α-Fe, (b) (100) planes, (c) (200) planes

As an example of absences due to lattice type, consider α-Fe. (Fig. 5.24a), which is body centred cubic. Reflection from the (100) planes (Fig. 5.24b) has zero intensity and is systematically absent. This is because, at the Bragg angle for these planes, the body centre atoms which lie midway between adjacent (100) planes diffract X-rays exactly 180° out of phase relative to the corner atoms which lie on the (100) planes. Averaged over the whole crystal, there are equal numbers of corner and body centre atoms and the beams diffracted by each cancel completely. In contrast, a strong 200 reflection is observed because all the atoms lie on (200) planes (Fig. 5.24c) and there are no atoms lying between (200) planes to cause destructive interference. It is easy to show, by similar arguments, that the 110 reflection is observed whereas 111 is systematically absent in α-Fe. For each non-primitive lattice type there is a simple characteristic formula for systematic absences (Table 5.5). For a body centred cell reflections for which $(h + k + l)$ is odd are absent, e.g. reflections such as 100, 111, 320, etc., are systematically absent.

Systematic absences caused by the presence of space symmetry elements are rather complicated and difficult to describe and will be dealt with only briefly. Absences arise because, in certain orientations of a crystal that possesses space symmetry elements, the dimensions of one or more of the unit cell edges appear to be reduced (often by half). For the screw axis shown in Fig. 5.17(a), the true cell repeat, a, is indicated; however, when the (h00) planes only are considered the cell repeat appears to be $a/2$. Because the (h00) planes are perpendicular to x, any

Table 5.5 *Systematic Absences due to lattice type*

Lattice type	Rule for reflection to be observed*
Primitive, P	None
Body centred, I	hkl; $h + k + l = 2n$
Face centred, F	hkl; h, k, l either all odd or all even
Side centred, e.g. C	hkl; $h + k = 2n$
Rhombohedral, R	hkl; $-h + k + l = 3n$ or $(h - k + l = 3n)$

* If space symmetry elements are present, additional rules limiting the observable reflections may apply.

difference in rotational orientation about x does not affect diffraction from the (h00) planes. In other words, the position of atoms in planes perpendicular to x does not affect the intensity of (h00) reflections since these intensities depend only on the atomic positions along the x axis. Thus, by considering diffraction from the (h00) planes alone, it is not possible to distinguish between a simple translation of $a/2$ and a translation of $a/2$ combined with a rotation of 180° about x. For a 2_1 screw axis parallel to x, reflections such as (100), (300),...,(h00): $h = 2n + 1$ are systematically absent.

It is difficult to show pictorially how the presence of glide planes leads to certain systematic absences. Suffice it to say that it does and that there are several types of glide plane, depending on the magnitude and direction of the translation step and on the orientation of the reflection plane. For example, a glide plane which has a translation of $b/2$ and is reflected across the bc plane is characterized by the absence of reflections of the type $0kl : k = 2n + 1$; i.e. for the $0kl$ planes the length of the b cell edge appears to be halved. Further discussion of screw axes and glide planes is given in Chapter 6.

5.3.10 Multiplicities

For cubic materials, lattice planes such as (013), (031), (103), (130), etc., all have the same d-spacing, as can be shown readily from the d-spacing formula for cubic crystals (equation 5.5). In a powder X-ray pattern, the variable coordinate is d-spacing, or Bragg angle θ, and, therefore, reflections which have the same d-spacing will be superposed. The multiplicity of a powder line is the number of lines, one from each set of planes, that are superposed to give the observed line. Multiplicities may be calculated readily if the crystal symmetry is known: the object is to find the maximum possible number of (hkl) combinations which are equivalent, taking both positive and negative values of h, k and l. The maximum multiplicity possible is 48 and occurs for cubic symmetry and h, k, l reflections where $h \neq k \neq l \neq 0$; i.e.

hkl	$h\bar{k}l$	hlk	$h\bar{l}k$	lkh	$l\bar{k}h$
$hk\bar{l}$	$h\bar{k}\bar{l}$	$hl\bar{k}$	$h\bar{l}\bar{k}$	$lk\bar{h}$	$l\bar{k}\bar{h}$
$h\bar{k}l$	$\bar{h}\bar{k}l$	$h\bar{l}k$	$\bar{h}\bar{l}k$	$l\bar{k}h$	$\bar{l}\bar{k}h$
$\bar{h}kl$	$\bar{h}\bar{k}\bar{l}$	$\bar{h}lk$	$\bar{h}\bar{l}\bar{k}$	$\bar{l}kh$	$\bar{l}\bar{k}\bar{h}$
lhk	$l\bar{h}\bar{k}$	klh	$k\bar{l}\bar{h}$	khl	$k\bar{h}\bar{l}$
$lh\bar{k}$	$l\bar{h}k$	$kl\bar{h}$	$k\bar{l}h$	$kh\bar{l}$	$k\bar{h}l$
$l\bar{h}k$	$\bar{l}hk$	$k\bar{l}h$	$\bar{k}lh$	$k\bar{h}l$	$\bar{k}hl$
$\bar{l}hk$	$\bar{l}h\bar{k}$	$\bar{k}lh$	$\bar{k}l\bar{h}$	$\bar{k}hl$	$\bar{k}h\bar{l}$

For orthorhombic crystals, h, k and l cannot be interchanged, as $a \neq b \neq c$, but negative and positive permutations are still possible to give a general multiplicity

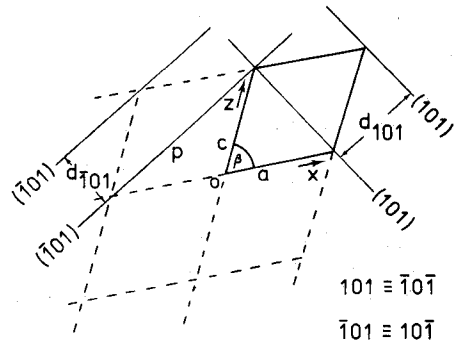

Fig. 5.25 Negative and positive Miller indices

of eight; i.e.

hkl	$hk\bar{l}$	$h\bar{k}l$	$\bar{h}kl$
$h\bar{k}\bar{l}$	$\bar{h}k\bar{l}$	$\bar{h}\bar{k}l$	$\bar{h}\bar{k}\bar{l}$

The number of possible permutations for any symmetry is reduced when h, k or $l = 0$. For example, the cubic 100 powder line has a multiplicity of only six, i.e. 100, $\bar{1}00$, 010, $0\bar{1}0$, $00\bar{1}$ and $00\bar{1}$. Orthorhombic 100 has a multiplicity of two, i.e. 100 and $\bar{1}00$.

Negative Miller indices indicate that the opposite or negative directions of the relevant axes must be used in defining the Miller indices. This is seen in Fig. 5.25 which shows a monoclinic cell, as heavy lines, in projection down b. The origin of the cell, O, and the chosen positive directions for x and z are marked. For illustration consider the {101} planes. These planes are all parallel to y and, therefore, perpendicular to the plane of the paper. Two planes of the sets (101) and ($\bar{1}$01) are drawn as light lines. In defining the ($\bar{1}$01) planes, the plane p, which is the plane adjacent to the one (not shown) that passes through the origin, cuts the x axis at -1 and the z axis at 1. It should be apparent from the scale of the drawing that $d_{101} \neq d_{\bar{1}01}$ unless $\beta = 90°$, as in, say, orthorhombic crystals.

The ($\bar{1}0\bar{1}$) planes (not shown) are exactly the same as the (101) planes and may simply be regarded as the (101) planes 'looked at from the opposite direction'. It is important, however, to give the (101) and ($\bar{1}0\bar{1}$) planes separate status, especially in single crystal diffraction studies. Similarly, the planes ($\bar{1}$01) and (10$\bar{1}$) are the same but are treated separately in diffraction. For general planes, (hkl), this equality or 'counting twice' of d-spacings is for the pairs of planes (hkl) and ($\bar{h}\bar{k}\bar{l}$). All powder lines therefore have a minimum multiplicity of two. In single crystal diffraction studies (hkl) and ($\bar{h}\bar{k}\bar{l}$) may be observed as separate reflections. The intensity of corresponding (hkl) and ($\bar{h}\bar{k}\bar{l}$) reflections is usually the same but under certain circumstances, such as when *anomalous dispersion* is present, the intensities are not equal. It is often stated that 'diffraction patterns in reciprocal space possess a centre of symmetry'. This grandiose statement means that hkl and

$\bar{h}\bar{k}\bar{l}$ reflections are equivalent, subject to the condition that anomalous dispersion is not present.

5.3.11 Unit cell contents, crystal densities and formulae

The unit cell, by definition, must contain at least one formula unit, whether it be an atom, ion pair, molecule, etc. In centred cells, and sometimes in primitive cells, the unit cell contains more than one formula unit. A simple relation may be derived between the cell volume, the number of formula units in the cell, the formula weight and the bulk crystal density. The density is given by

$$D = \frac{\text{mass}}{\text{volume}} = \frac{\text{formula weight}}{\text{molar volume}}$$

$$= \frac{\text{FW}}{\text{volume of formula unit} \times N}$$

where N is Avogrado's number. If the unit cell, of volume V, contains Z formula units, then

$$V = \text{volume of one formula unit} \times Z$$

Therefore,

$$D = \frac{\text{FW} \times Z}{V \times N} \tag{5.6}$$

V is usually expressed as Å^3 and must be multiplied by 10^{-24} to give densities in the normal units of grams per cubic centimetre. Substituting for Avogrado's number, the above formula reduces to

$$D = \frac{\text{FW} \times Z \times 1.66}{V} \tag{5.7}$$

If V is in Å^3 in equation (5.7), the units of D are in grams per cubic centimetre.

This simple formula has a number of uses, as shown by the following examples:

(a) It can be used to check that a given set of crystal data are consistent and that, for example, an erroneous formula weight has not been assumed.
(b) It can be used to determine any of the four variables if the other three are known. This is most common for Z (which must be a whole number) but is also used to determine FW and D.
(c) By comparison of D_{obs} (the experimental density of a material) and $D_{X\text{-ray}}$ (the density calculated from the above formula), information may be obtained on: the presence of crystal defects such as vacancies as opposed to interstitials, the mechanisms of solid solution formation, the porosity of ceramic pieces.

Considerable confusion often arises in determining the value of the contents, **Z**, of a unit cell. This is because atoms or ions that lie on corners, edges or faces of the unit cell are also shared between adjacent cells, and this must be taken into consideration.

For example, α-Fe (Fig. 5.24a) has $Z = 2$. The corner iron atoms, of which there are eight, are each shared between eight neighbouring unit cells. Effectively, each contributes only $\frac{1}{8}$ to the particular cell in question, giving $8 \times \frac{1}{8} = 1$ net iron atom for the corners. The body centre iron atom lies entirely inside the unit cell and counts as one. Hence $Z = 2$.

For NaCl (Fig. 5.9), $Z = 4$, i.e. $4(Na^+ Cl^-)$. The corner Na^+ ions again count as one. The face centre Na^+ ions, of which there are six, count as $\frac{1}{2}$ each, giving a total of $1 + 3 = 4\,Na^+$ ions. The Cl^- ions at the edge centres, of which there are twelve, count as $\frac{1}{4}$ each, which, together with Cl^- at the body centre, give a total of $12 \times \frac{1}{4} + 1 = 4\,Cl^-$ ions.

5.4 The X-ray diffraction experiment

When reduced to basic essentials, the X-ray diffraction experiment, Fig. 5.26, requires an X-ray source, the sample under investigation and a detector to pick up the diffracted X-rays. Within this broad framework, there are three variables which govern the different X-ray techniques:

(a) radiation—monochromatic or of variable λ;
(b) sample—single crystal, powder or a solid piece;
(c) detector—radiation counter or photographic film.

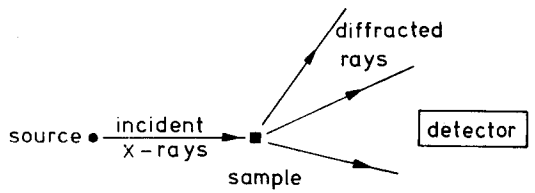

Fig. 5.26 The X-ray diffraction experiment

WAVELENGTH	*SAMPLE*	*DETECTOR*	*METHOD*
Fixed	Powder	Counter	Diffractometer
		Film	Debye-Scherrer
			Guinier (Focusing)
	Single crystal	Film	Rotation (Oscillation)
			Weissenberg
			Precession (Buerger)
		Counter	Automatic Diffractometer
Variable	Solid piece	Film	Laue

Fig. 5.27 The different X-ray diffraction techniques

These are summarized for the most important techniques in Fig. 5.27. With the exception of the Laue method, which is used almost exclusively by metallurgists and is not discussed here, monochromatic radiation is nearly always used. An outline of powder and single crystal methods is given in this section with a more comprehensive account of powder methods being given in Section 5.6.

5.4.1 The powder method—principles and uses

The principles of the powder method are shown in Fig. 5.28. A monochromatic beam of X-rays strikes a finely powdered sample that, ideally, has crystals randomly arranged in every possible orientation. In such a powder sample, the various lattice planes are also present in every possible orientation. For each set of planes, therefore, at least some crystals must be oriented at the Bragg angle, θ, to the incident beam and thus, diffraction occurs for these crystals and planes. The diffracted beams may be detected either by surrounding the sample with a strip of photographic film (Debye–Scherrer and Guinier focusing methods) or by using a movable detector, such as a Geiger counter, connected to a chart recorder (diffractometer).

The original powder method, the *Debye–Scherrer method*, is little used

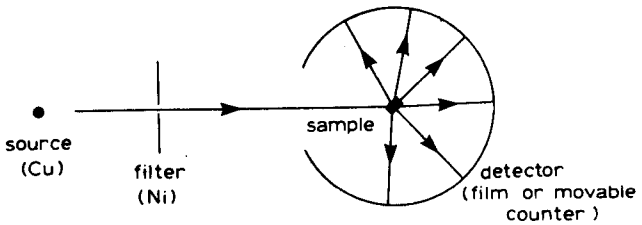

Fig. 5.28 The powder method

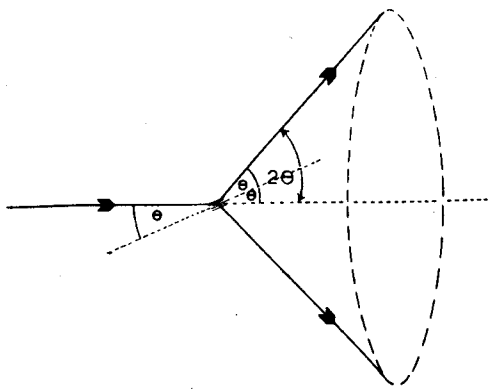

Fig. 5.29 The formation of a cone of diffracted radiation in the powder method

nowadays, but since it is simple it is instructive to consider its mode of operation. For any set of lattice planes, the diffracted radiation forms the surface of a cone, as shown in Fig. 5.29. The only requirement for diffraction is that the planes be at angle θ to the incident beam; no restriction is placed on the angular orientation of the planes about the axis of the incident beam. In a finely powdered sample, crystals are present at every possible angular position about the incident beam and the diffracted beams that result appear to be emitted from the sample as cones of radiation. (Each cone is in fact a large number of closely spaced diffracted beams.) If the Bragg angle is θ, then the angle between diffracted and undiffracted beams is 2θ and the angle of the cone is 4θ. Each set of planes gives its own cone of radiation. The cones are detected by a thin strip of film wrapped around the sample (Fig. 5.28); each cone intersects the film as two short arcs (Fig. 5.30), which are symmetrical about the two holes in the film (these allow entry and exit of incident and undiffracted beams). In a well-powdered sample, each arc appears as a continuous line, but in coarser samples the arcs may be spotty due to the relatively small number of crystals present.

To obtain d-spacings from the Debye–Scherrer film, the separation, S, between pairs of corresponding arcs is measured. If the camera (film) radius, R, is known, then

$$\frac{S}{2\pi R} = \frac{4\theta}{360} \tag{5.8}$$

from which 2θ and therefore d may be obtained for each pair of arcs. The disadvantages of this method are that exposure times are long (6 to 24 hours) and that closely spaced arcs are not well resolved. This is because, although the incident beam enters the camera through a pinhole slit and collimator tube, the beam is somewhat divergent and the spread increases in the diffracted beams. If, in an effort to increase the resolution, a finer collimator is used, the resulting diffracted beams have much less intensity and longer exposure times are needed. Apart from considerations of the extra time involved, the amount of background radiation detected by the film (as fogging) increases with exposure time and, consequently, weak lines may be lost altogether in the background.

In modern film methods (*Guinier focusing methods*) a *convergent*, intense incident beam is used with the result that excellent resolution of lines is obtained and exposure times are much reduced (10 min to 1 hr). A convergent beam is obtained by placing a bent single crystal of quartz or graphite between the X-ray source and the sample. The orientation of this bent crystal is adjusted so that it

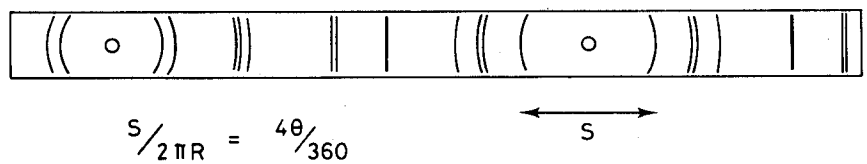

Fig. 5.30 Schematic Debye–Scherrer photograph

diffracts the incident beam and converts it from a divergent beam into a convergent one. The beam then strikes the sample and the diffracted beams are arranged to focus at the surface of the film. Further details are given in Section 5.6. A typical schematic, Guinier film is shown in Fig. 3.1.

The other modern powder technique is *diffractometry*, which gives a series of peaks on a strip of chart paper. A convergent incident beam is again used (Section 5.6) to give fairly good resolution of peaks. Both peak positions and intensities (peak heights) are readily obtained from the chart to make this a very useful and rapid method of phase analysis.

The most important use of the powder method is in the qualitative identification of crystalline phases or compounds. While most chemical methods of analysis give information about the *elements* present in a sample, powder diffraction is very different and perhaps unique in that it tells which *crystalline compounds* or *phases* are present but gives no direct information about their chemical constitution.

Each crystalline phase has a characteristic powder pattern which can be used as a fingerprint for identification purposes. The two variables in a powder pattern are peak position, i.e. d-spacing, which can be measured very accurately if necessary, and intensity, which can be measured either qualitatively or quantitatively. It is rare but not unknown that two materials have identical powder patterns. More often, two materials have one or two lines with common d-spacings, but on comparing the whole patterns, which may contain between ~ 5 and 100 observed lines, the two are found to be quite different. In more extreme cases, two substances may happen to have the same unit cell parameters and, therefore, the same d-spacings, but since different elements are probably present in the two, their intensities are quite different. The normal practice in using powder patterns for identification purposes is to pay most attention to the d-spacings but, at the same time, check that the intensities are roughly correct.

For the identification of unknown crystalline materials, an invaluable reference source is the *Powder Diffraction File* (Joint Committee on Powder Diffraction Standards, Swarthmore, USA), previously known as the ASTM file, which contains the powder patterns of about 35000 materials; new entries are added at the current rate of ~ 2000 p.a. In the search indices, materials are classified either according to their most intense peaks or according to the first eight lines in the powder pattern in order of decreasing d-spacing. Identification of an unknown is usually possible within 30 min of obtaining its measured powder pattern. Problems arise if the material is not included in the file (obviously!) or if the material is not pure but contains lines from more than one phase.

For many types of work, the materials being analysed may not be completely unknown but may be restricted to a range of possible phases. It is then much easier to have to hand a standard pattern of all the phases likely to be encountered. Comparison of the unknown with the standard patterns leads to identification in a matter of minutes. Guinier films are admirably suited to this type of work since they are small and can be easily compared by simply lining up the back stop mark (corresponding to $0° 2\theta$) on each.

Table 5.6 *Some uses of the powder method*

Characterization of materials by X-ray 'fingerprints'
Qualitative phase analysis (presence or absence of phases)
Quantitative phase analysis
Refinement of unit cell parameters
Study of solid solution formation
Determination of crystal size
Study of crystal distortion by stress
Measurement of thermal expansion coefficients (HTXR)*
Determination of high temperature phase diagrams (HTRX)*
Study of phase transformations
Crystal structure determination
Study of the reactions of solids

* HTXR = high temperature X-ray diffraction.

The powder method has many important secondary uses, especially in the general area of applied crystallography. These are discussed in Section 5.6 and in various places throughout this book; a summary is given in Table 5.6.

5.4.2 Single crystal methods—principles and uses

The main uses of single crystal methods are, as indicated in Section 3.2.1.3, to determine unit cells and space groups and, if there is sufficient interest, to measure the intensities of reflections and carry out a full crystal structure determination. Monochromatic X-rays are generally used, an optimum crystal size is ~ 0.2 mm diameter and the detector may be either film or counter. Only film methods are discussed here. The sole purpose of the counter method, using a single crystal diffractometer, is to collect intensity data. As such it is an extremely valuable instrument but it is not really a technique which a solid state chemist can use for himself as part of his armoury of experimental techniques and, therefore, is not discussed further.

There are three main film techniques: the rotation or oscillation method, the Weissenberg method and the precession method. A brief outline of each is given next but details of how the instruments work are omitted. The latter two methods are rather complicated and anyone wishing to understand them is recommended to get direct instruction and practical experience in their use.

In the *rotation method*, a crystal is mounted by sticking it onto, for example, a

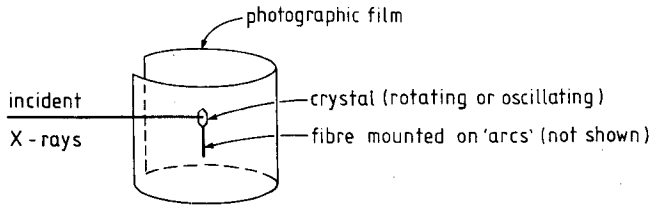

Fig. 5.31 Schematic single crystal rotation method

glass fibre. The crystal is *set* so that one of its unit cell axes is vertical and it is made to oscillate or rotate about this axis (Fig. 5.31). A horizontal beam of X-rays strikes the crystal and the diffracted beams are detected by a piece of film bent round the crystal in the form of a cylinder. After developing the film, parallel rows of spots are seen (Fig. 5.32), each spot corresponding to diffraction from one particular set of planes in the crystal. There are two main uses of these photographs. From oscillation photographs (with the crystal oscillated through, for example, 15° about the vertical axis), the presence of symmetry in the distribution and intensity of spots in the photograph is looked for. In particular, if the top half of the photograph is a mirror image of the bottom half, as it is in Fig. 5.32, then the vertical axis, about which the crystal is set, is an axis of symmetry. Not all unit cell axes are symmetry axes. For instance, in an orthorhombic structure all three axes are symmetry axes but in a monoclinic structure, only the unique *b* axis is a symmetry axis. The second use is for determining the magnitude of the unit cell dimension in the vertical direction. Although this is straightforward, a special chart is needed in order to measure the distance between adjacent rows of spots. This distance in *reciprocal space* is inversely related to the magnitude of the unit cell dimension in *real space*. Thus, if the rows are closely spaced the unit cell dimension is large, and vice versa.

Let us consider briefly how the *zero layer* in Fig. 5.32 arises. The zero layer is the row that passes through the centre of the film. Suppose the crystal has orthorhombic symmetry and is set with *c* vertical; *a* and *b* are therefore horizontal. From the definition of Miller indices, we know that planes of the type (*hk*0) have one direction in common in that they are all parallel to *c*. Since the incident X-ray beam is horizontal and therefore perpendicular to *c*, it follows that all beams diffracted from the (*hk*0) planes are also horizontal. These beams radiate horizontally from the crystal and are detected on film as the zero layer row of spots.

The next row of spots, the *first layer*, corresponds to reflections from the (*hk*1) set of planes, and so on. The position of the spots on the zero layer row depends

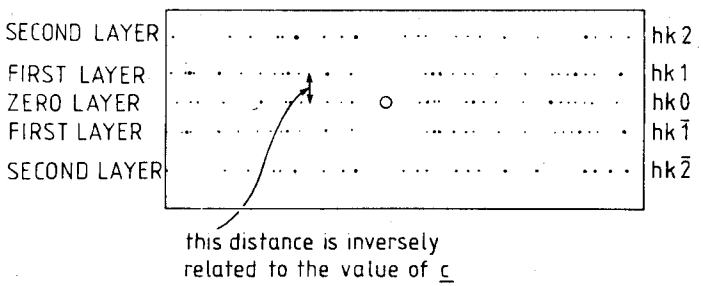

Fig. 5.32 Schematic oscillation photograph obtained in the rotation method. It is assumed that the crystal *c* axis is vertical. Further details are not given since a reference chart is needed in order to measure up the photograph

on the *d*-spacings of the planes in question and therefore on the values of *h* and *k*. Planes that have large *d*-spacings diffract X-rays at low Bragg angles and these are the spots closest to the hole in the centre of the film (this hole is the exit for undiffracted X-rays and corresponds to a Bragg angle of zero).

In studying a new crystal, one usually starts with the rotation camera. Once the crystal is set with one axis vertical, it is possible to tell from the photographs the value of that unit cell dimension. To obtain the remaining cell dimensions (two sides, three angles), the individual rows of spots have to be analysed. If the crystal is of high symmetry and does not give too many spots on the rotation photograph, it may be possible to obtain the remaining information by a suitable graphical analysis of the photograph. It is more common, however (if one has the equipment), to put the crystal onto either a Weissenberg or a precession camera. Essentially, both of these cameras take a single row of spots (as observed in the rotation photograph) and separate the spots into two dimensions.

In the *Weissenberg method*, the crystal is also surrounded cylindrically by film but metal screens are placed between the crystal and the film such that only one row of spots, or layer line, is allowed through. During exposure, the crystal undergoes a slow oscillation and at the same time the film translates up and

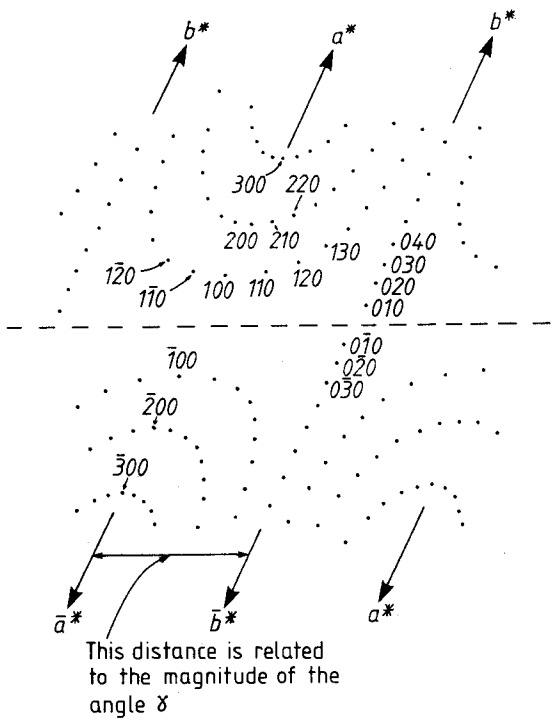

Fig. 5.33 Schematic zero layer (*hk*0) Weissenberg photograph. All spots are shown with equal intensity. In practice, intensities vary

down. The coupling of the film and crystal motions is rather complicated and will not be considered here. A schematic, simplified Weissenberg photograph is shown in Fig. 5.33. The pattern of spots is distorted because of the manner of the coupling between the two motions. From the photograph, one first looks for the two axes; these are labelled as a^* and b^* if the crystal is set about c; note that each axis appears on the photograph several times. (The starring of axes is associated with the reciprocal lattice; it is discussed later and in Appendix 7.) The axial spots lie on straight lines but all the others are on curves. The separation of the spots along the a^* and b^* axes is related inversely to the value of the cell parameter for those axes and so the second and third unit cell dimensions may be obtained from the photographs. The distance between two axial rows of spots is related to the angle between these two axes in the unit cell, i.e. to the angle γ for axes a^* and b^*. Because of the distorted nature of Weissenberg photographs it is almost essential, in measuring them up, to superpose the film over a suitably scaled reference grid (not shown). It then becomes a straightforward process to obtain the relevant unit cell information. Some of the spots in Fig. 5.33 have been assigned Miller indices, hkl. The method used for this assignment is similar to that used for precession photographs, discussed next.

The *precession method* gives photographs that are much easier to interpret and measure and also are more attractive aesthetically (see Fig. 3.2 and Section 3.2.1.3). Each layer line of a rotation photograph is converted, in a precession photograph, into a two-dimensional network of spots. One first inspects the photograph for the presence of symmetry in the distribution and intensity of the spots and thereby locates the two axes a^* and b^* (sometimes it is possible to choose more than one set of valid axes, especially if there is not much symmetry evident from the photograph). Next, it is important (in Weissenberg films also) to assign Miller indices to the spots. To see how this is done, let us suppose that our

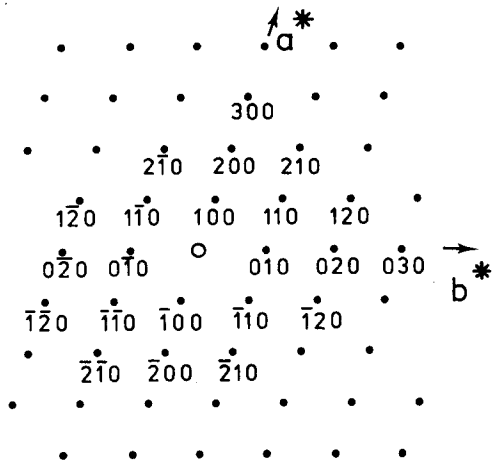

Fig. 5.34 Indexing of a precession photograph, $hk0$ layer

photograph is a zero layer photograph for a crystal set about c (Fig. 5.34) and for which the angle between a^* and b^* is not 90°. All the spots, therefore, have Miller indices that belong to the set ($hk0$). The spots are shown of the same size and intensity but in practice this is most unlikely to occur. The spots in the row that forms the a^* axis have indices ($h00$) which are labelled, working out from the centre of the film, with increasing h values. Similarly, the row of spots that forms the b^* axis is the ($0k0$) set of reflections and is labelled accordingly. Negative directions of a^* and b^* are indicated by the bar over the appropriate Miller indices. We have now labelled the two axes and so all remaining spots may be indexed, as shown.

A fundamental feature of precession photographs is that distances on them, e.g. between pairs of spots, are inversely proportional to the corresponding distances in the actual crystal. Consider the $h00$ reflections. We know that $d_{100} = 2d_{200} = 3d_{300}$, etc. On the precession photograph, the reverse is true. The distance of the 100 spot from the origin (the centre of the film) is exactly half the distance of the 200 spot from the origin, and so on. This brings us to the distinction between *real space*, in which the crystal exists, and *reciprocal space*, which describes the directions followed by diffracted beams and hence the patterns of spots on single crystal photographs. The starring of axes, a^* and b^*, is done to distinguish the axes of the *reciprocal lattice* from those of their real space counterparts, a and b. If the unit cell in real space is orthogonal ($\alpha = \beta = \gamma = 90°$), then real and reciprocal axes are parallel because, for example, $\alpha^* = 180° - \alpha = 90° = \alpha$, etc. This is not necessarily true for non-orthogonal crystals, however, if $\alpha^* \neq \alpha$, etc. A derivation of the reciprocal lattice is given in Appendix 7.

The beauty of the precession method is that, unlike the Weissenberg method, its photographs give an undistorted picture of the reciprocal lattice. This makes their interpretation very easy and logical. A slight disadvantage is that the theory behind the operation of the camera is rather complicated.

The use of single crystal methods in determining the nature of the unit cell and its dimensions has been mentioned several times. An extension of this is the determination of lattice type and possible space group(s) by inspecting the Weissenberg or precession photographs for systematically absent reflections. Once Miller indices have been assigned to spots, it is easy to see if certain groups of spots are absent (remember, centred lattices, screw axes and glide planes all cause systematic absences). For example, the arrangement of spots in Fig. 5.35(a) shows that the a^* row has every other spot absent in the $hk0$ layer; let us assume that there are no systematic absences in the $hk1$ layer (not shown). From this, we can say that there are no general $hk1$ absences and no general $hk0$ absences, but for $h00$ we have the condition that, for reflection to occur, $h = 2n$ (because 100, 300, 500, etc., are absent). This means that parallel to a in the crystal, there is a 2_1 screw axis.

In Fig. 5.35(b) and (c) are shown schematic zero layer and first layer photographs for a body centred lattice. From an examination of (b) in isolation one would perhaps choose 1 and 2 for axes of the reciprocal lattice but it would then be difficult to subsequently interpret (c) because in (c) no spots lie on the axes,

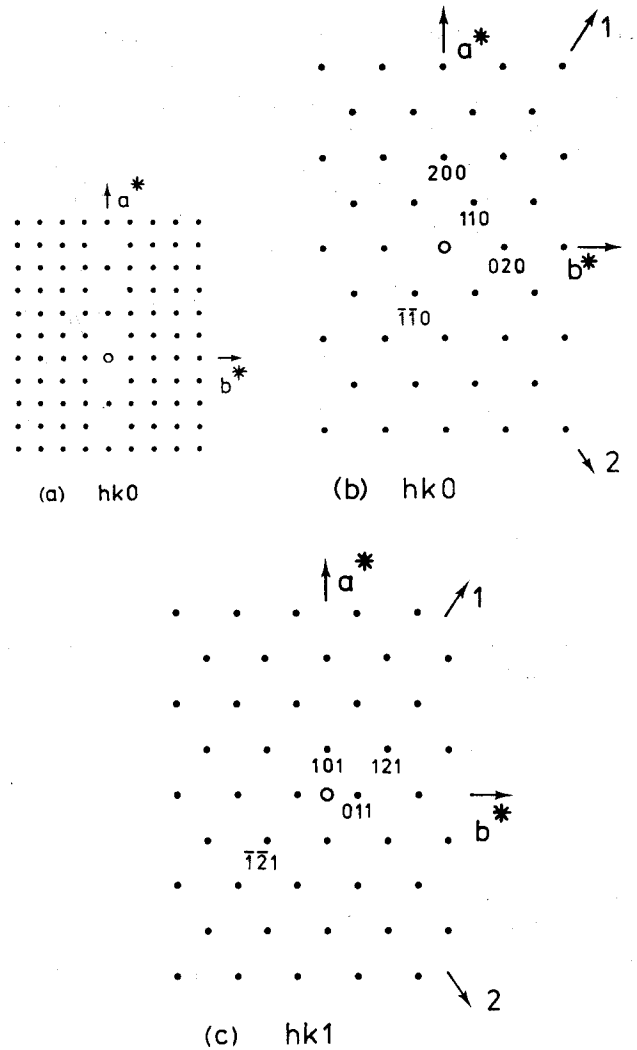

Fig. 5.35 Reciprocal lattices showing (a) 2_1 screw axis parallel to *a*, (b) and (c) body centring

1 and 2. The correct axes are marked a^* and b^*; in (b) alternate spots are systematically absent which leads to the condition for reflection; $hk0$: $h + k = 2n$ (e.g. 200, 400, 110, 130, etc., are present). In (c) also, alternate spots are absent but now the condition for reflection is $hk1$: $h + k = 2n + 1$ (e.g. 101, 011, 211, etc., are present). If we assume that layers $hk2$, $hk4$, etc., have the same pattern of absences as $hk0$ and that $hk3$, $hk5$, etc., are similar to $hk1$, then we arrive at the general condition for reflection hkl: $h + k + l = 2n$, which corresponds to a body centred lattice type, Table 5.5. The reader may now like to work out how a face centred lattice appears in reciprocal space. The answer is given in Appendix 7.

Once the crystal system, lattice type and systematic absences have been determined, a short list of possible space groups—sometimes one, but, more usually, two or three—for the crystal can be found by comparing the absences with those for the different space groups (given in *International Tables for X-Ray Crystallography*, Vol. 1). For example, suppose our crystal has a primitive orthorhombic unit cell and its only systematic absences indicate a 2_1 screw axis parallel to one of the unit cell axes. From an inspection of all possible space groups we find that our crystal must belong to the space group $P222_1$ (Chapter 6).

5.5 Intensities

Intensities of X-ray reflections are important for two main reasons. First, quantitative measurements of intensity are necessary in order to determine unknown crystal structures. Second, qualitative or semi-quantitative intensity data are needed in using the powder fingerprint method to characterize materials and especially in using the powder diffraction file to identify unknowns. Although this book is not concerned with the methods of crystal structure determination, it is considered important that the factors which control the intensity of X-ray reflections be understood. The topic falls into two parts: the intensity scattered by individual atoms and the resultant intensity scattered from the large number of atoms that are arranged periodically in a crystal.

5.5.1 Scattering of X-rays by an atom

Atoms diffract or scatter X-rays because an incident X-ray beam, which can be described as an electromagnetic wave with an oscillating electric field, sets each electron of an atom into vibration. A vibrating charge such as an electron emits radiation and this radiation is in phase or *coherent with* the incident X-ray beam. The electrons of an atom therefore act as secondary point sources of X-rays. Coherent scattering may be likened to an elastic collision between the wave and the electron: the wave is deflected by the electron without loss of energy and, therefore, without change of wavelength. The intensity of the radiation scattered coherently by 'point source' electrons has been treated theoretically and is given by the Thomson equation:

$$I_p \alpha \tfrac{1}{2}(1 + \cos^2 2\theta) \qquad (5.9)$$

where I_p is the scattered intensity at any point, P, and 2θ is the angle between the directions of the incident beam and the diffracted beam that passes through P. From this equation it can be seen that the scattered beams are most intense when parallel or antiparallel to the incident beam and are weakest when at 90° to the incident beam. The Thomson equation is also known as the *polarization factor* and is one of the standard angular correction factors that must be applied during the processing of intensity data (for use in structure determination).

At this point, it is worth mentioning that X-rays can interact with electrons in a different way to give *Compton scattering* (Section 5.6.8). Compton scattering is

rather like an elastic collision in that the X-rays lose some of their energy on impact and so the scattered X-rays are of longer wavelength than the incident X-rays. They are also no longer in phase with the incident X-rays; nor are they in phase with each other. A close similarity exists between Compton scattering and the generation of white radiation in an X-ray tube; both are examples of incoherent scattering that are sources of background radiation in X-ray diffraction experiments. As Compton scattering is caused by interaction between X-rays and the more loosely held outer valence electrons, it is an important effect with the lighter elements and can have a particularly deleterious effect on the powder patterns of organic materials such as polymers.

The X-rays that are scattered by an atom are the resultant of the waves scattered by each electron in the atom. The electrons may be regarded as particles that occupy different positions in an atom and interference occurs between their scattered waves. For scattering in the direction of the incident beam (Fig. 5.36a) beams 1′ and 2′, all electrons scatter in phase irrespective of their position. The scattered intensity is, then, the sum of the individual intensities. The *scattering factor*, or *form factor*, f, of an atom is proportional to its atomic number, Z, or, more strictly, to the number of electrons possessed by that atom.

For scattering at some angle 2θ to the direction of the incident beam, a phase difference, corresponding to the distance XY, exists between beams 1″ and 2″. This phase difference is usually rather less than one wavelength (i.e. XY < 1.5418 Å for Cu $K\alpha$ X-rays) because distances between electrons within an atom are short. As a result, only partial destructive interference occurs between 1″ and 2″. The net effect of interference between the beams scattered by all the electrons in the atom is to cause a gradual decrease in scattered intensity with increasing angle, 2θ. For example, the scattering power of copper is proportional to 29 (i.e. Z) at $2\theta = 0°$, to 14 at 90° and to 11.5 at 120°. It should also be apparent from Fig. 5.36(a) that for a given angle, 2θ, the net intensity decreases with decreasing X-ray wavelength. The form factors of atoms are given in *International Tables for X-ray Crystallography*, Vol. 3 (1952). They are tabulated against $(\sin\theta/\lambda)$ to include the effect of both angle and X-ray wavelength; examples are shown in Fig. 5.36(b).

Two consequences of the dependence of form factors on $\sin\theta/\lambda$ and atomic number are as follows. First, the powder patterns of most materials contain only weak lines at high angles (above ~60 to 70° 2θ). Although several factors contribute to powder intensities, the main reason for this effect is that the atoms scatter only weakly at high angles (Fig. 5.36b). Second, in crystal structure determinations using X-rays, it is difficult to locate light atoms because their diffracted radiation is so weak. Thus hydrogen atoms cannot usually be located unless all the other elements present are also extremely light (e.g. in boron hydride crystals). Atoms that have as many electrons as oxygen can usually be located easily unless a very heavy atom such as uranium is present. Structures that are particularly difficult to solve are those in which a considerable number or all of the atoms present have similar atomic number, e.g. large organic molecules with carbon, nitrogen and oxygen atoms. In such cases, a common ploy is to make a

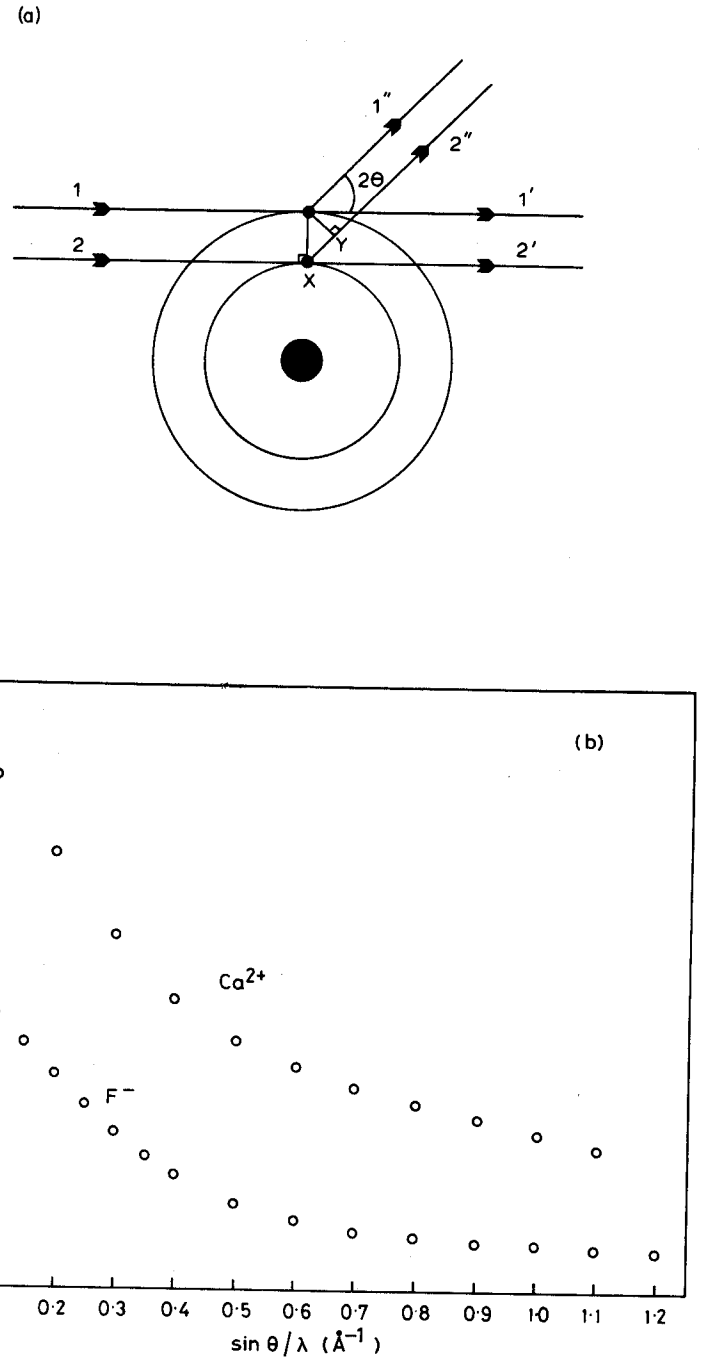

Fig. 5.36 (a) Scattering of X-rays by electrons in an atom. (b) Form factors of Ca^{2+} and F^-

derivative of the compound of interest which contains a heavy metal atom. The heavy atoms can be detected very readily and because they determine the phase of diffracted beams, a lead is given towards placing the remaining atoms. Because of their similar atomic numbers, aluminium and silicon are very difficult to distinguish, which causes problems in determinations of aluminosilicate structures. One of the advantages of using neutrons instead of (or as well as) X-rays for crystallographic work is that the neutron form factors are not a simple function of atomic number. Light atoms, e.g. hydrogen and lithium are often strong neutron scatterers (Section 3.2.1.5).

5.5.2 Scattering of X-rays by a crystal

Each atom in a material acts as a secondary point source of X-rays. If the material is non-crystalline, beams are scattered by the atoms in all directions, but in crystalline materials the scattered beams interfere destructively in most possible directions. In other directions, interference is constructive or only partially destructive, resulting in the X-ray beams that are detected in diffraction experiments. The amount of interference and hence the resultant intensity depend on the relative phases of the beams scattered by each atom and therefore on the atomic positions in the crystal structure.

In Section 5.3.9, the phenomenon of systematically absent reflections is treated. Examples are given where both lattice centring and the presence of elements of space symmetry cause sets of reflections to be absent. The treatment is now extended to consider some special examples of partially destructive interference followed by consideration of general expressions for intensities.

Consider the rock salt structure. It is face centred cubic and, therefore, only those reflections may be observed for which *hkl* are either all odd or all even (Table 5.5). From this rule, for instance, 110 is systematically absent but 111 may be observed. Both of these planes are shown for NaCl in Fig. 5.37. In Fig. 5.37(a), (110) planes have Na^+ and Cl^- ions lying on the planes and equal numbers of the same ions lying midway between the planes. Complete cancellation of the 110

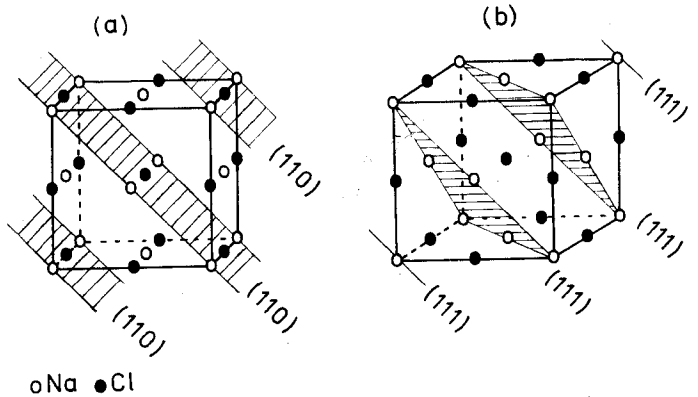

Fig. 5.37 (a) (110) and (b) (111) planes in NaCl

Table 5.7 *X-ray powder diffraction patterns for potassium halides.* (Data from Joint Committee on Powder Diffraction Standards, Swarthmore)

	KF, $a = 5.347$ Å		KCl, $a = 6.2931$ Å		KI, $a = 7.0655$ Å	
(*hkl*)	*d*(Å)	*I*	*d*(Å)	*I*	*d*(Å)	*I*
111	3.087	29		—	4.08	42
200	2.671	100	3.146	100	3.53	100
220	1.890	63	2.224	59	2.498	70
311	1.612	10	—	—	2.131	29
222	1.542	17	1.816	23	2.039	27
400	1.337	8	1.573	8	1.767	15

reflection therefore occurs. In Fig. 5.37(b), (111) planes have Na^+ ions lying on the planes and Cl^- ions midway between the planes. The Na^+ and Cl^- ions scatter exactly 180° out of phase with each other for these planes, but since they have different scattering powers the destructive interference that occurs is only partial. The intensity of the 111 reflection in materials that have the rock salt structure is, therefore, related to the difference in atomic number of anion and cation. For the potassium halides, the 111 intensity is zero for KCl, since K^+ and Cl^- are isoelectronic, and its intensity should increase in the order

$$KCl < KF < KBr < KI$$

Some data which confirm this are given in Table 5.7.

Similar effects may be found in other simple crystal structures. In primitive cubic CsCl, if the difference between cesium and chlorine is ignored the atomic positions are the same as in body centred α-Fe (Fig. 5.24). The 100 reflection is systematically absent in α-Fe but is an observed reflection with CsCl because the scattering powers of Cs^+ and Cl^- are different, i.e. $f_{Cs^+} \neq f_{Cl^-}$.

5.5.3 Intensities—general formulae and a model calculation for CaF_2

Each atom in a crystal scatters X-rays by an amount related to the scattering power, *f*, of that atom. In summing the individual waves to give the resultant diffracted beam, both the *amplitude* and *phase* of each wave are important. If we know the atomic positions in the structure, the amplitude and phase appropriate to each atom in the unit cell may be calculated and the summation carried out by various mathematical methods, therefore simulating what happens during diffraction. Let us consider first the relative phases of different atoms in the unit cell. In Fig. 5.38(a) are drawn two (100) planes of a crystal that has an orthogonal (i.e. $\alpha = \beta = \gamma = 90°$) unit cell. The atoms A, B, C, A′ lie on the *a* axis (perpendicular to (100) planes) with A and A′ at the origin of adjacent unit cells. For the 100 reflection, A and A′ scatter in phase because their phase difference is exactly one wavelength, 2π radians (Bragg's Law). Atom B, situated halfway between adjacent (100) planes, has a fractional *x* coordinate (relative to A) of $\frac{1}{2}$. The phase difference between (waves diffracted from) A and B is $\frac{1}{2} \cdot 2\pi = \pi$, i.e. atoms

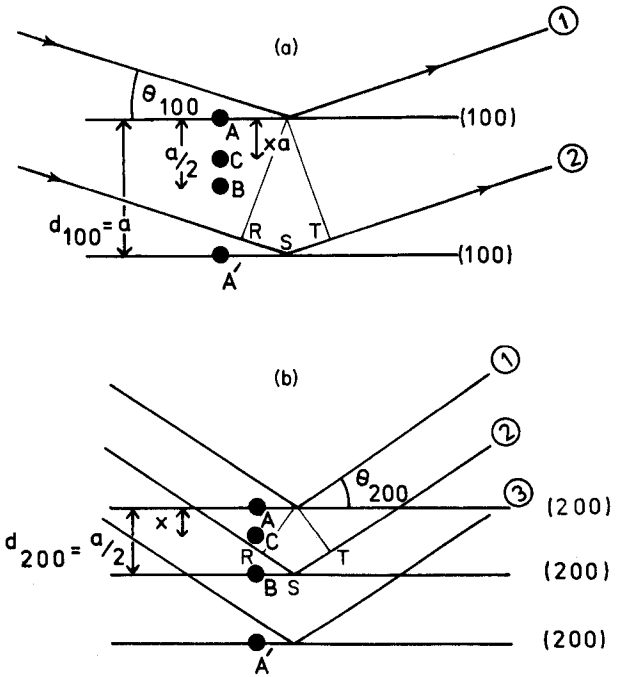

Fig. 5.38 (a) (100) planes for an orthogonal unit cell ($\alpha = \beta = \gamma = 90°$). Atoms A, B, C, A′ lie on the a cell edge. (b) (200) planes for the same unit cell as in (a)

A and B are exactly out of phase. Atom C has a general fractional coordinate x (at distance xa from A) and, therefore, a phase relative to A of $2\pi x$.

Consider, now, the 200 reflection for the same unit cell (Fig. 5.38b). Atoms A and B have a phase difference of 2π for the 200 reflection and scatter in phase, whereas their phase difference is π for the 100 reflection (in order to obey Bragg's Law, if d is halved, $\sin\theta$ must double; thus $\theta_{200} \geqslant \theta_{100}$). Comparing the Bragg diffraction conditions for the (100) and (200) planes, the effect of halving d is to double the relative phase difference between pairs of atoms such as A and B; therefore, A and C have a phase difference of $(2x \cdot 2\pi)$ for the (200) reflection.

For the general case of an $h00$ reflection, the d-spacing between adjacent $(h00)$ planes is $(1/h)a$ (for an orthogonal cell); the phase difference, δ, between A and C is given by

$$\delta = 2\pi hx \tag{5.10}$$

The phase difference between atoms depends, therefore, on two factors: the Miller indices of the reflection that is being considered and the fractional coordinates of the atoms in the unit cell. The above reasoning may be extended readily to the general three-dimensional situation. For reflection from the set of planes with indices (hkl), the phase difference, δ, between atoms at the origin and a position

with fractional coordinates (x, y, z) is given by

$$\delta = 2\pi(hx + ky + lz) \tag{5.11}$$

This is an important formula and is applicable to all unit cell shapes. Let us use it on a simple structure, γ-Fe, which is face centred cubic with atoms at the corner and face centre positions, i.e. with fractional coordinates:

$$(0,0,0); \quad (\tfrac{1}{2},\tfrac{1}{2},0); \quad (\tfrac{1}{2},0,\tfrac{1}{2}); \quad (0,\tfrac{1}{2},\tfrac{1}{2})$$

These coordinates may be substituted into the formula for δ to give four phases:

$$0, \quad \pi(h+k), \quad \pi(h+l), \quad \pi(k+l)$$

How do these vary with the Miller indices? If h, k and l are either all even or all odd, the phases are in multiples of 2π and, therefore, are in phase with each other.

If, however, one, say h, is odd and the other two, k and l, are even, the four phases reduce to

$$0, \quad (2n+1)\pi, \quad (2n+1)\pi, \quad 2n\pi$$

The first and last are π out of phase with the middle two and complete cancellation occurs. The γ-Fe structure is a simple example of a face centred cubic lattice in which the iron atoms correspond to lattice points and, in fact, we have just proved the condition for systematic absences due to face centring (Table 5.5). The reader may like to prove the condition for systematic absences in a body centred cubic structure, e.g. by working out the phases of the atoms for the structure of α-Fe.

The second major factor that affects intensities is the amplitude of the individual waves scattered by each atom as given by the scattering power, f. From Section 5.5.1, f is proportional to atomic number, Z, and decreases with increasing Bragg angle, θ.

We now wish to generalize the treatment to consider any atom in the unit cell. For atom j, the diffracted wave of amplitude f_j and phase δ_j may be represented by a sine wave of the form

$$F_j = f_j \sin(\omega t - \delta_j) \tag{5.12}$$

The waves diffracted from each atom in the cell have the same angular frequency, ω, but may differ in f and δ. The resultant intensity is obtained from the summation of the individual sine waves. Mathematically, addition of waves may be carried out by various methods, including vector addition and by the use of complex numbers. In complex notation, wave j may be written as

$$F_j = f_j(\cos\delta_j + i\sin\delta_j) \tag{5.13}$$

or as

$$F_j = f_j e^{i\delta_j} \tag{5.14}$$

The intensity of a wave is proportional to the square of its amplitude; i.e.

$$I \propto f_j^2 \tag{5.15}$$

and is obtained by multiplying the equation for the wave by its complex conjugate; i.e.

$$I \propto (f_j e^{i\delta_j})(f_j e^{-i\delta_j})$$

and, therefore

$$I \propto f_j^2$$

Alternatively,

$$[f_j(\cos\delta_j + i\sin\delta_j)][f_j(\cos\delta_j - i\sin\delta_j)] = f_j^2(\cos^2\delta_j + \sin^2\delta_j) = f_j^2$$

Substituting the expression for δ, the equation of a diffracted wave becomes

$$\begin{aligned} F_j &= f_j \exp 2\pi i(hx_j + ky_j + lz_j) \\ &= f_j[\cos 2\pi(hx_j + ky_j + lz_j) + i\sin 2\pi(hx_j + ky_j + lz_j)] \end{aligned} \tag{5.16}$$

When written in these forms, the summation over the j atoms in the unit cell may be carried out readily, to give the *structure factor* or *structure amplitude*, F_{hkl}, for the *hkl* reflection; i.e.

$$F_{hkl} = \sum_{j=1-n} (f_j e^{i\delta j})$$

or

$$F_{hkl} = \sum_j f_j(\cos\delta_j + i\sin\delta_j) \tag{5.17}$$

The intensity of the diffracted beam I_{hkl} is proportional to $|F_{hkl}|^2$ and is obtained from

$$I_{hkl} \alpha |F_{hkl}|^2 = \left[\sum_j f_j(\cos\delta_j + i\sin\delta_j)\right]\left[\sum_j f_j(\cos\delta_j - i\sin\delta_j)\right]$$

$$= \sum_j (f_j\cos\delta_j)^2 + \sum_j (f_j\sin\delta_j)^2 \tag{5.18}$$

This latter is a very important formula in crystallography because by using it the intensity of any *hkl* reflection may be calculated from a knowledge of the atomic coordinates in the unit cell. Let us see one example of its use. Calcium fluoride, CaF_2, has the fluorite structure with atomic coordinates in the face centred cubic unit cell:

Ca	$(0,0,0)$	$(\frac{1}{2},\frac{1}{2},0)$	$(\frac{1}{2},0,\frac{1}{2})$	$(0,\frac{1}{2},\frac{1}{2})$
F	$(\frac{1}{4},\frac{1}{4},\frac{1}{4})$	$(\frac{1}{4},\frac{1}{4},\frac{3}{4})$	$(\frac{1}{4},\frac{3}{4},\frac{1}{4})$	$(\frac{3}{4},\frac{1}{4},\frac{1}{4})$
	$(\frac{3}{4},\frac{3}{4},\frac{1}{4})$	$(\frac{3}{4},\frac{1}{4},\frac{3}{4})$	$(\frac{1}{4},\frac{3}{4},\frac{3}{4})$	$(\frac{3}{4},\frac{3}{4},\frac{3}{4})$

Substitution of these coordinates into the structure factor equation, (5.18), yield

$$\begin{aligned} F_{hkl} = {} & f_{Ca}[\cos 2\pi(0) + \cos\pi(h+k) + \cos\pi(h+l) + \cos\pi(k+l)] \\ & + if_{Ca}[\sin 2\pi(0) + \sin\pi(h+k) + \sin\pi(h+l) \\ & + \sin\pi(k+l)] + f_F[\cos\pi/2(h+k+l) \\ & + \cos\pi/2(h+k+3l) + \cos\pi/2(h+3k+l) \\ & + \cos\pi/2(3h+k+l) + \cos\pi/2(3h+3k+l) \\ & + \cos\pi/2(3h+k+3l) + \cos\pi/2(h+3k+3l) \\ & + \cos\pi/2(3h+3k+3l)] + if_F[\sin\pi/2(h+k+l) \\ & + \sin\pi/2(h+k+3l) + \sin\pi/2(h+3k+l) + \sin\pi/2(3h+k+l) \\ & + \sin\pi/2(3h+3k+l) + \sin\pi/2(3h+k+3l) \\ & + \sin\pi/2(h+3k+3l) + \sin\pi/2(3h+3k+3l)] \end{aligned}$$

Since the fluorite structure is face centred cubic, *h*, *k* and *l* must be either all odd or all even for an observed reflection; for any other combination, $F = 0$ (try it!). Consider the reflection 202:

$$\begin{aligned} F_{202} = {} & f_{Ca}(\cos 0 + \cos 2\pi + \cos 4\pi + \cos 2\pi) \\ & + if_{Ca}(\sin 0 + \sin 2\pi + \sin 4\pi + \sin 2\pi) \\ & + f_F(\cos 2\pi + \cos 4\pi + \cos 2\pi + \cos 4\pi + \cos 4\pi + \cos 6\pi \\ & + \cos 4\pi + \cos 6\pi) + if_F(\sin 2\pi + \sin 4\pi + \sin 2\pi + \sin 4\pi + \sin 4\pi \\ & + \sin 6\pi + \sin 4\pi + \sin 6\pi) \end{aligned}$$

That is,

$$\begin{aligned} F_{202} = {} & f_{Ca}(1+1+1+1) + if_{Ca}(0+0+0+0) \\ & + f_F(1+1+1+1+1+1+1+1) \\ & + if_F(0+0+0+0+0+0+0+0) \end{aligned}$$

or

$$F_{202} = 4f_{Ca} + 8f_F$$

The 202 reflection in CaF_2 has a *d*-spacing of 1.929 Å ($a = 5.464$ Å). Therefore

$$\theta_{202} = 23.6° \quad \text{and} \quad \sin\theta/\lambda = 0.259 \quad \text{for } \lambda = 1.5418\,\text{Å (Cu } K\alpha)$$

Form factors for calcium and fluorine are given in Fig. 5.36(b); for $\sin\theta/\lambda = 0.259$, by interpolation,

$$f_{Ca} = 12.65 \quad \text{and} \quad f_F = 5.8$$

Therefore,

$$F_{202} = 97$$

This calculation may be made for a series of *hkl* reflections and the results, after scaling, may be compared with the observed values (Table 5.8). In solving unknown crystal structures, the objective is always to obtain a model structure for which the calculated structure factors, F_{hkl}^{calc}, are in good agreement with those obtained from the experimental intensities, i.e. F_{hkl}^{obs}.

An important feature which simplifies the above calculations is that all the sine terms are zero. This is because the origin of the unit cell is also a centre of symmetry. For each atom at position (x, y, z) there is a centrosymmetrically

Table 5.8 *Structure factor calculations for* CaF_2

d(Å)	hkl	I	Multiplicity	I/(multiplicity × L_p)	F^{obs}	F^{calc}	F^{obs} scaled	$\|\|F^{obs}\| - \|F^{calc}\|\|$
3.143	111	100	8	0.409	0.640	67	90	23
1.929	202	57	12	0.476	0.690	97	97	0
1.647	311	16	24	0.098	0.313	47	44	3
1.366	400	5	6	0.193	0.439	75	62	13
1.254	331	4	24	0.047	0.217	39	31	8

$\sum F^{obs}$ scaled = 324

$\sum |F^{obs} - F^{calc}| = 47$

$$R = \frac{\sum |\Delta F|}{\sum F^{obs}} = \frac{47}{324} = 0.15$$

related atom at $(-x, -y, -z)$ [e.g. F at $(\frac{1}{4},\frac{1}{4},\frac{1}{4})$ and $(-\frac{1}{4}-\frac{1}{4}-\frac{1}{4})$, i.e. $(1-\frac{1}{4}, 1-\frac{1}{4}, 1-\frac{1}{4})$ or $(\frac{3}{4},\frac{3}{4},\frac{3}{4})$] and since $\sin(-\delta) = -\sin\delta$, the summation of the sine terms over the unit cell contents is zero. If, on the other hand, one of the F atoms was taken as the origin of the cell, the sine terms would be non-zero because, F, with its immediate coordination environment of 4Ca arranged tetrahedrally, does not lie on a centre of symmetry. Many structures, of course, belong to non-centric space groups, in which case the complete calculation of F using both cosine and sine terms cannot be avoided.

A further discussion of Table 5.8 is deferred to Section 5.5.5.

5.5.4 Factors that affect intensities

Intensities depend on several factors and not only on the structure factor discussed above. The main factors are:

(a) Polarization factor—angular dependence of intensity scattered by electrons (Section 5.5.1).

(b) Structure factor—dependence on the position of atoms in the unit cell and their scattering power (Section 5.5.3).

(c) Lorentz factor—a geometric factor that depends on the particular type of instrument used and varies with θ. Usually lumped with (a) to give the L_p *factor* (given in International Tables for X-ray Crystallography, Vol. 2, 266–90).

(d) Multiplicities—the number of reflections that contribute to an observed powder line (Section 5.3.10).

(e) Temperature factor—thermal vibrations of atoms cause a decrease in the intensities of diffracted beams and an increase in background scatter (Section 5.6.8).

(f) Absorption factor—absorption of X-rays by the sample and depends on the form of the sample and geometry of the instrument. Ideally, for single crystal work, crystals should be spherical so as to have the same absorption factor in all directions.

(g) Preferred orientation—occurs if the samples used in powder diffraction do not have a completely random arrangement of crystal orientations (Sections 5.4.1 and 5.6.1).

(h) Extinction—crystals that are nearly perfect have a reduced diffracting power, unimportant in powders.

These factors need to be considered quantitatively only if one is interested in carrying out work related to crystal structure determinations. For usage of (a) single crystal methods to determine unit cells and (b) powder methods to fingerprint materials, it is normal practice to use the raw intensity data without applying any of these correction factors.

5.5.5 *R*-factors and structure determination

In Section 5.5.3, it was shown how the structure factor, F_{hkl}^{calc}, may be calculated for any *hkl* reflection from a knowledge of the coordinates of the atoms in the unit

cell. The values of F_{hkl}^{calc} for the first five lines in the powder pattern of CaF_2 are given in Table 5.8, column 7. The experimental intensities are given in column 3 and the intensities after correction for the L_p factor and multiplicities (Section 5.5.4(a), (c) and (d) in column 5. The observed structure factor, F_{hkl}^{obs}, is related to the corrected intensities by the relation: $F_{hkl}^{obs} = \sqrt{I_{corr}}$, and these values are given in column 6. In order to be able to compare the values of F_{hkl}^{obs} and F_{hkl}^{calc}, they must be scaled such that $\sum F_{hkl}^{obs} = \sum F_{hkl}^{calc}$. Multiplication of each F_{hkl}^{obs} value by 141 gives the scaled values in column 8. The measure of agreement between the individual, scaled F_{hkl}^{obs} and F_{hkl}^{calc} values is given by the *residual factor* or *R-factor*, defined as follows:

$$R = \frac{\sum ||F^{obs}| - |F^{calc}||}{\sum |F^{obs}|} \qquad (5.19)$$

Values of the numerator are listed in column 9 and an R-factor of 0.15 (or 15 per cent after multiplying by 100) is obtained.

In solving unknown crystal structures, one is guided, among other things, by the value of R; the lower it is, the more likely is the structure to be correct. The calculation given for CaF_2 is rather artificial since only five reflections were used (one normally uses hundreds or thousands of reflections), but it serves as an illustration. It is not possible to give hard and fast rules about the relation between the magnitude of R and the likely correctness of the structure, but, usually, when R is less than 0.1 to 0.2, the proposed structure is essentially correct. A structure which has been solved fully using good quality intensity data has R typically in the range 0.02 to 0.06.

5.5.6 Electron density maps

An electron density map is a plot of the variation of electron density throughout the unit cell. During the processes of solving an unknown structure it is often useful to construct electron density maps (Fourier maps) in order to try and locate atoms. As the structure refinement proceeds, the quality of the electron density map usually improves: the background electron density decreases and, at the same time, more peaks due to individual atoms become resolved. We are concerned here, not with the methods of structure refinement but only with the results, and the final electron density map obtained at the end of a structure determination is an important piece of information. Electron density maps usually take the form of sections through the structure at regular intervals; by superposing these, a three-dimensional picture of the electron density distribution may be obtained. In Fig. 5.39 is shown the electron density distribution for a section through a very simple structure, NaCl. The section is parallel to one face of the unit cell and passes through the centres of the Na^+, Cl^- ions. It has the following features.

An electron density map resembles a geographical contour map. The contours represent lines of constant electron density throughout the structure. Peaks of electron density maxima may be distinguished clearly and these correspond to

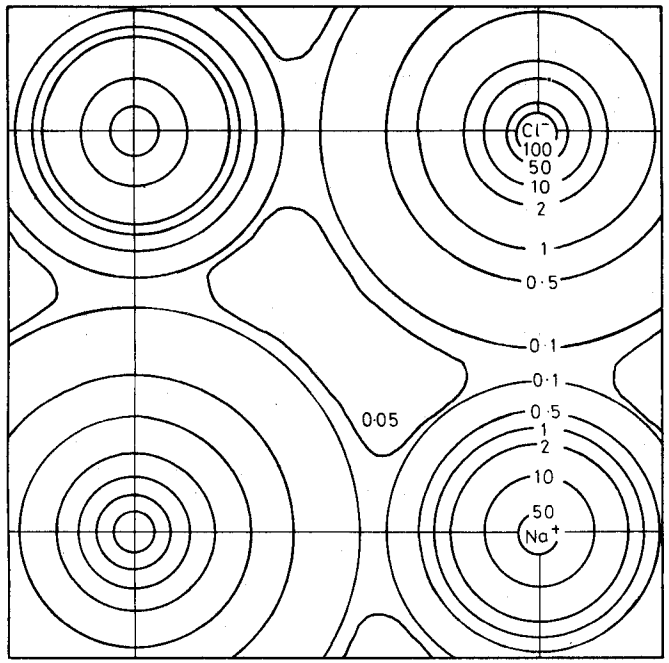

Fig. 5.39 Electron density map for NaCl

atoms; the coordinates of the atoms in the unit cell are given by the coordinates of the peak maxima. The assignment of peaks to particular atoms is made from the relative heights of the electron density peaks: the peak height is proportional to the number of electrons possessed by that atom, which apart from very light atoms is approximately equal to the atomic number of that atom. In Fig. 5.39, two types of peak of relative heights 100 and 50, are seen; these are assigned to chlorine and sodium, respectively. (The atomic numbers of chlorine and sodium are 17 and 11; for ions, the number of electrons are 18 (Cl^-) and 10(Na^+). The experimental maxima are therefore in fair agreement with the expected values.)

Electron density maps also show that our mental picture of atoms as spheres is essentially correct, at least on a time average. The electron density drops to almost zero at some point along the line connecting pairs of adjacent atoms in Fig. 5.39 and this supports the model of ionic bonding in NaCl. In other structures which have covalent bonding, there is residual electron density between atoms on the electron density map. However, in other than very simple structures, such as the alkali halides, there is one serious difficulty in using an electron density map to determine quantitatively the distribution of valence electrons. In most structure refinements, both the position and thermal vibration factors of atoms are allowed to vary in order to achieve the best agreement between measured and calculated structure factors and intensities. The final parameters may represent a compromise, therefore, and the electron density map, which is greatly influenced by the thermal vibration factors, is not necessarily a

true representation of the distribution of valence electrons. In refining more simple structures, the atomic coordinates are usually known exactly; this gives rather more accuracy to the thermal vibration factors (or temperature factors) and hence to the electron density map.

5.6 Modern X-ray powder techniques and their applications

5.6.1 Powder diffractometers

The most commonly used powder X-ray instrument is the powder diffractometer. Its mode of operation is outlined in Section 5.4.1. It has a proportional, scintillation or Geiger counter as the detector which is connected to a chart recorder or sometimes to a means of digital output. In normal use, the counter is set to scan over a range of 2θ values at a constant angular velocity (it is common practice to refer to the angle 2θ between diffracted and undiffracted beams, rather than to the Bragg angle, θ). Usually, the range 10 to 80° 2θ is sufficient to cover the most useful part of the powder pattern. A typical diffractometer trace is shown in Fig. 18.6a for SiO_2. The scale is linear in 2θ and the d-spacings of the peaks may be calculated from Bragg's Law or obtained from standard tables of d versus 2θ. The scanning speed of the counter is usually $2° 2\theta\,\text{min}^{-1}$ and, therefore, about 30 min are needed to obtain a trace. Intensities are taken as peak heights, unless very accurate work is being done, in which case areas may be measured; the most intense peak is given intensity of 100 and the rest are scaled accordingly.

If very accurate d-spacings or intensities are desired, slower scanning speeds (e.g. $\frac{1}{8}° 2\theta\,\text{min}^{-1}$) are used. To obtain accurate d-spacings, an internal standard (a pure material, such as KCl, whose d-spacings are known accurately) is mixed in with the sample. A correction factor, which may vary with 2θ, is obtained from the discrepancy between observed and true d-spacings of the standard and is then applied to the pattern that is being measured. Accurate intensities are obtained from peak areas by cutting out the peaks and weighing them, by measuring their area with a device such as a planimeter or by using an automatic counter fitted to the diffractometer.

Samples for diffractometry take various forms: they include thin layers of the fine powder sprinkled onto a glass slide smeared with vaseline and thin flakes pressed onto a glass slide. Different people prefer different methods of sample preparation and the objective is always to obtain a sample which contains a random arrangement of crystal orientations. If the crystal arrangement is not random, then *preferred orientation* exists and can introduce errors, sometimes very large, into the measured intensities. Preferred orientation is a serious problem for materials that crystallize in a characteristic, very non-spherical shape, e.g. clay minerals which usually occur as thin plates or some cubic materials which crystallize as cubes and, on crushing, break up into smaller cubes. In a powder aggregate of such materials, the crystals tend to sit on their faces, resulting in a far from random average orientation.

The big disadvantage of early Debye–Scherrer cameras is that incident and

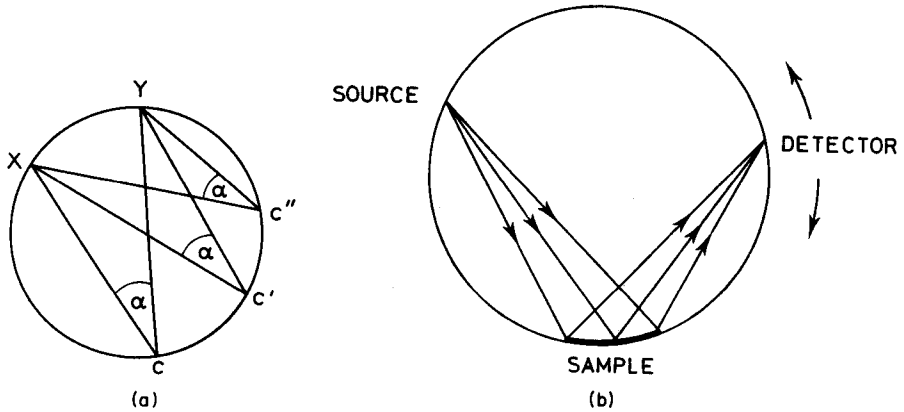

Fig. 5.40 (a) Theorem of a circle used to focus X-rays. (b) Arrangement of sample, source and detector on the circumference of a circle

diffracted beams are, inevitably, somewhat divergent and of low intensity. In diffractometers and modern focusing cameras, a convergent X-ray beam is used; this gives a dramatic improvement in resolution and, because much more intense beams may be used, exposure times are greatly reduced. It is not possible to focus or converge X-rays using the X-ray equivalent of an optical lens; instead, use is made of certain geometric properties of the circle in order to obtain a convergent X-ray beam. These properties are illustrated in Fig. 5.40(a). The arc XY forms part of a circle and all angles subtended on the circumference of this circle by the arc XY are equal, i.e. XCY = XC′Y = XC″Y = α. Suppose that X is a source of X-rays and XC, XC′ represent the extremities of a divergent X-ray beam emitted from X. If the beam is diffracted by a sample which covers the arc between C and C′ such that the diffracting planes are tangential to the circle, then the diffracted beam, represented by CY and C′Y, will focus to a point at Y. The principle of the focusing method is therefore to arrange that the source of X-rays, the sample and the detector all lie on the circumference of a circle (Fig. 5.40b).

The focusing geometry of the diffractometer is shown schematically in Fig. 5.41. The *focusing circle* is dashed and has the source, S, sample and the receiving slit of the detector at F, all on its circumference. The focusing circle is not of constant size but decreases in radius as the Bragg angle θ increases (movement of F around the diffractometer circle with increasing θ is indicated by the arrow). The importance of having a flat sample surface can be seen (ideally it should be curved and change its radius of curvature with scanning angle, but this is not practicable); if the surface is uneven, or deviates much from the circumference of the circle, then the focusing action is lost.

The solid circle in Fig. 5.41 is the *diffractometer circle* and is of constant size. The sample is at its centre and the detector, F, scans around its circumference. In order to preserve the focusing action with changing 2θ, the surface of the sample must stay tangential to the focusing circle. This is achieved by coupling the

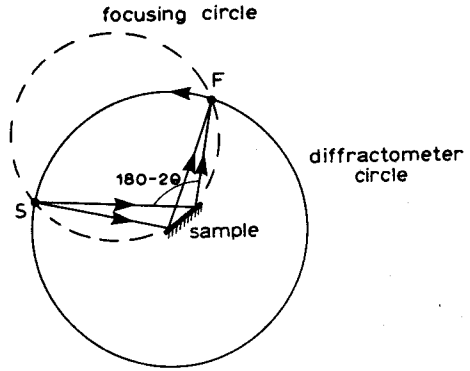

Fig. 5.41 Focusing geometry of the diffractometer

sample to the detector so that as the detector scans at angular velocity $2\theta\,\text{min}^{-1}$, the sample rotates in the same direction at $\theta\,\text{min}^{-1}$.

5.6.2 Focusing (Guinier) cameras

The same focusing principle that is basic to the construction of diffractometers is also used in focusing cameras, although several different arrangements are found in commercial instruments. An addition feature of focusing cameras is the inclusion of a *crystal monochromator* which serves two functions: to give highly monochromatic radiation and to produce an intense, convergent X-ray beam. There are several sources of background scattering in diffraction experiments (Section 5.6.8), one of which is the presence of radiation of wavelength different from that of the $K\alpha$ radiation. $K\alpha$ radiation may be separated from the rest by the use of filters or, better, by a crystal monochromator.

A crystal monochromator consists of a large single crystal of, for example, quartz, oriented such that one set of planes which diffracts strongly ($10\bar{1}1$ for quartz) is at the Bragg angle to the incident beam. This Bragg angle is calculated for $\lambda_{K\alpha_1}$ and so only the $K\alpha_1$ rays are diffracted, giving monochromatic radiation. (In fact, overtone reflections may occur because the $(20\bar{2}2)$ planes diffract X-rays of wavelength $\frac{1}{2}\lambda_{K\alpha}$ at the same Bragg angle. It is an easy matter to ensure that these overtone reflections have weak or negligible intensity.) If a flat crystal monochromator were used, much of the $K\alpha$ radiation would be lost since the X-ray beam emitted from a source is naturally divergent; only a small amount of the $K\alpha$ component would therefore be at the correct Bragg angle to the monochromator. To improve the efficiency, the crystal monochromator is bent, in which case a divergent X-ray beam may be used which is diffracted by the crystal monochromator to give a beam that is intense, monochromatic and convergent.

The arrangement of a focusing or Guinier camera which uses a crystal monochromator M and also makes use of the theorem of the circle described above is shown in Fig. 5.42. The convergent beam of monochromatic radiation

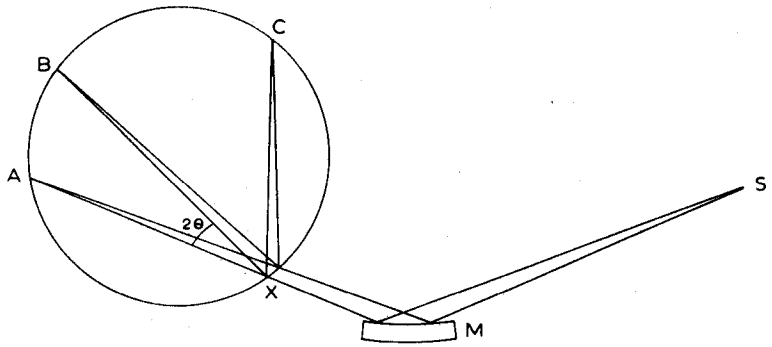

Fig. 5.42 Crystal monochromator M, source S and sample X, in a focusing camera

passes through the sample at X. Radiation that is not diffracted comes to a focus at A, where a beam stop is placed in front of the film to prevent its blackening. Various beams diffracted by the sample focus at B, C, etc. We know from the theorem of the circle that A, B, C and X must lie on the circumference of a circle. The film is placed in a cassette which is in the form of a short cylinder and lies on the circle ABC. The scale of the film is linear in 2θ, as is the chart output from a diffractometer. A schematic film is as shown in Fig. 3.1 except that instead of peaks of different height, lines of different intensity or different degrees of blackness are seen. Film dimensions are $\sim 1 \times 15\,\text{cm}$ which makes them very convenient to handle. The line at $0°\,2\theta$ or ∞ d-spacing corresponds to the undiffracted beam at A in Fig. 5.42. This is the reference position on the film. The mark is made by removing the beam stop for a fraction of a second while the X-rays are switched on. If required, a scale may be printed onto the film and the positions of the lines, relative to A, may be measured with a travelling microscope or, better, by microdensitometry; 2θ values and d-spacings may then be computed or obtained from tables.

The Guinier method is capable of giving accurate d-spacings, if desired, and the results are comparable to those obtained by diffractometry using very slow scanning speeds. Intensities of the lines on the films are either estimated visually or may be measured quantitatively using microdensitometry. Sample sizes are very small, 1 mg or less, and necessary exposure times vary between 5 min and 1 hr, depending on factors such as the crystallinity of the sample and the presence or absence of heavy elements which absorb X-rays.

5.6.3 Measurement of powder patterns and comparison of diffractometry with film methods

A powder pattern has three main features that may be measured quantitatively. In decreasing order of relative importance, these are (a) d-spacings, (b) intensities and (c) line profiles.

5.6.3.1 *d-spacings*

For routine measurements and for purposes of identification, no special care need be taken over sample preparation nor in the measurement of the film or diffractometer trace. For identification of completely unknown materials, diffractometry is probably quicker and somewhat easier. It is important to have approximate intensity values as well as reasonably accurate d-spacings and both may be determined directly from the diffractometer chart. Further, with film methods, there is a delay time of 1 to 2 hours during which the film is developed and prepared ready for examination.

The great advantage of film methods over diffractometry occurs when the powder patterns of different samples are to be compared. It is almost impossible to compare several 1 metre lengths of chart paper by trying to match or superpose the different traces. Yet with small Guinier films, several may be compared directly on a viewing screen. For work in specific areas, e.g. clay minerals, one can soon build up a file of standard films of all the phases likely to be encountered. Identification of unknowns and, probably more important, mixtures of unknowns then becomes straightforward and rapid.

For accurate measurement of d-spacings, diffractometry is normally regarded as the best method and most of the patterns in the powder diffraction file have been obtained by diffractometry. An internal standard of accurately known d-spacings must be added to the sample in order to eliminate instrumental error. A slow scanning speed, e.g. $\frac{1}{8}^\circ\ 2\theta\ \text{min}^{-1}$, is used so that the scale of the trace may be greatly expanded, and if possible only high angle reflections are used. A powder pattern obtained by either diffractometry or film methods is squashed up at its low angle end and hence accurate d-spacings are best measured in the back-reflection region using high angle reflections. Care must be taken that the diffractometer is well adjusted and that a smooth sample surface is presented to the incident beam so as to give good focusing action. The disadvantage of this method is that with the slow scanning speeds several hours may be needed to record a significant part of the powder pattern.

The superiority of diffractometry for accurate measurement of d-spacings is now being challenged by advances in focusing camera techniques. Both the position and intensity of lines may be determined from a microdensitometric scan of a Guinier film. The resulting d-spacings may be as accurate as those obtained by diffractometry and the process is much quicker: only a short exposure time is required to take the photograph, irrespective of the subsequent use that is made of the film.

5.6.3.2 *Intensities*

It is by no means a straightforward exercise to obtain reliable powder X-ray intensity data. Sample preparation is very important as it may be difficult if not impossible to avoid preferred orientation of crystals within the powder specimen. Powders should be ground down, preferably to size of 1 to 10 μm, and it may be worthwhile to sieve samples prior to X-ray diffraction. One or two large (e.g. 1 mm diameter) crystals in an otherwise fine powder can cause havoc with intensity measurements.

Table 5.9 *Comparison of diffractometers and focusing cameras*

Feature	Diffractometer	Focusing camera
Exposure time	30 min usually	10 min–1 hr
Accuracy of 2θ values	Good–very good	Good–very good
Intensities	Very good	Poor–fair
Peak shape	Very good	Poor–fair
Comparison of different samples	Poor (clumsy)	Excellent
Resolution of closely spaced lines	Good–excellent	Excellent
Amount of sample required	0.05–2 g	~ 1 mg
Storage and retrieval of results	Clumsy, unless done by computer	Easy
Approximate cost of equipment (excluding generator)	£15000	£5000

For comparison purposes the following were used: 1020 diffractometer; Hägg focusing camera (both Philips).

Intensities are normally measured by diffractometry, as peak heights or peak areas at slow scanning speeds. It is difficult to obtain quantitative intensities from films unless a microdensitometer is also available.

5.6.3.3 *Peak shape (line profiles)*

For certain specialized applications, the shape of peaks may yield valuable information. Peaks have a finite breadth, for reasons to be discussed later, but extra broadening may occur if (a) stresses are present in the crystals, e.g. in metal pieces that have been cold worked (Section 5.6.6), or (b) the size of the crystals is less than about 2000 Å diameter (Section 5.6.5). The standard method for measuring peak profiles is diffractometry.

The relative merits of diffractometers and focusing cameras are summarized in Table 5.9.

5.6.4 High temperature powder diffraction

Several commercial instruments are available for recording powder patterns at high temperatures. Some are diffractometers fitted with a small furnace around the sample. The powder pattern is recorded in exactly the same way as for room temperature operations. Inert, refractory construction materials such as tungsten and iridium are used and very high temperatures, e.g. 2000 °C, are attainable.

Film methods are also available and a particularly elegant one is the Guinier–

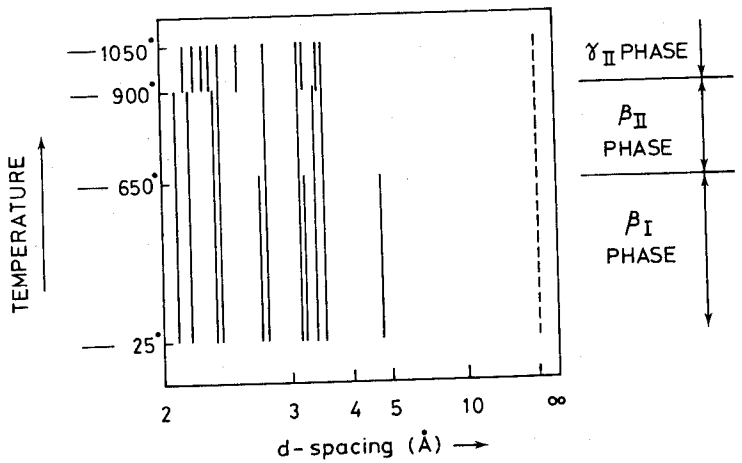

Fig. 5.43 Schematic high temperature Guinier powder photograph of Li_2ZnSiO_4

Lenne camera which operates up to $\sim 1200\,^{\circ}C$. A thin powdered specimen, mounted on a fine platinum gauze is suspended in the middle of a small furnace. A quartz crystal monochromator is used to provide a convergent X-ray beam and the diffraction pattern is recorded on film by the focusing method. The sample and furnace may be programmed to heat or cool at a certain rate and a continuous X-ray photograph is taken. The film is rectangular and bent to lie on the focusing circle (cylinder) of the camera. It can be translated at a constant velocity such that only a narrow strip of film, e.g. 5 mm wide, is exposed to the diffracted X-ray beams at any one time. A schematic photograph showing the polymorphic changes that occur on heating Li_2ZnSiO_4 is shown in Fig. 5.43. The horizontal axis is 2θ or d-spacing, as usual, and the vertical axis is temperature. One advantage of this particular camera is that because a continuous record is obtained, it is possible to follow phase transformations directly. This is often more useful than having two separate patterns that had been recorded before and after the changes involved took place.

Let us briefly consider the changes that appear on the photograph. With increasing temperature, the sequence $\beta_I \xrightarrow{650\,^{\circ}C} \beta_{II} \xrightarrow{900\,^{\circ}C} \gamma_{II}\ Li_2ZnSiO_4$ is observed. For the $\beta_I \rightarrow \beta_{II}$ transition, some of the lines in the β_I powder pattern simply disappear to give the powder pattern of β_{II}. Such a transition is characteristic of order–disorder phenomena (in this case, the ordering is probably orientational ordering of MO_4 tetrahedra) in which the low temperature phase is an ordered superstructure of the disordered high temperature phase. The $\beta_{II} \rightarrow \gamma_{II}$ transition is rather different in that some of the β_{II} lines disappear and new lines appear in the γ_{II} powder pattern. This indicates that some major structural reorganization occurs during the transition. The discontinuity in some of the lines indicates that a change in volume accompanies the $\beta_{II} \rightarrow \gamma_{II}$ transition and allows us to classify the transition thermodynamically as first order (see Chapter 12).

High temperature powder diffraction is invaluable for identifying and studying phases that exist only at high temperatures. Many phases, e.g. β-quartz stable above 573 °C, undergo a phase change during cooling (to α-quartz) and no matter how fast the cooling rate, the transition cannot be suppressed. The only way to study such phases is, therefore, at high temperatures.

A more technical application of high temperature powder diffraction is in the measurement of coefficients of thermal expansion, data which for some materials may be very difficult to obtain using conventional dilatometry. For non-cubic crystals, the expansion is usually anisotropic and the different axial expansion coefficients may be determined readily by the X-ray method. Knowledge of expansion coefficients is very important for materials that are used in high temperature environments or which experience large temperature changes during use, e.g. some metals and ceramics.

5.6.5 Effect of crystal size on the powder pattern—particle size measurement

If the average crystal size in a powder is below a certain limit (~ 2000 Å diameter), additional broadening of diffracted X-ray beams occurs. From measurement of this extra broadening an average particle size may be obtained. In the absence of extra broadening due to small particle size, powder lines or peaks have a finite breadth for several reasons: the radiation is not absolutely monochromatic, the $K\alpha$ line has an intrinsic breadth due to the Heisenberg uncertainty principle and the focusing geometry of the instrument may not be perfect for a variety of reasons. In order to understand why small particle size leads to line broadening it is necessary to consider the conditions under which diffraction may occur if the incident angle is slightly different from the Bragg angle, θ_B. A qualitative explanation is as follows.

The Bragg angle represents the condition under which each plane in a crystal diffracts exactly one wavelength later than the preceding plane. All diffracted beams are therefore in phase and constructive interference occurs. For an incident beam at a slightly greater angle, θ_1 (Fig. 5.44), there is a phase lag of slightly greater than one wavelength, $\lambda + \delta\lambda$, for rays diffracted from subsequent planes. By the time the $(j+1)$th plane is reached, let the cumulative, incremental

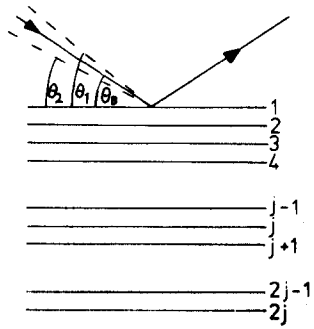

Fig. 5.44 Broadening of X-ray reflections due to small particle size

phase lag $\sum \delta\lambda$, be equal to half a wavelength; i.e.

$$j\delta\lambda = \lambda/2$$

Planes 1 and $(j+1)$ are exactly π out of phase for radiation that is incident and diffracted at θ_1 and, therefore, cancel each other. If the crystal contains a total of $2j$ planes, then the net diffracted intensity at θ_1 is equal to zero because the rays diffracted from planes $1 \rightarrow j$ exactly cancel the rays diffracted from planes $(j+1) \rightarrow 2j$. The angular range θ_B to θ_1 is the range over which the intensity of the diffracted beam falls from a maximum, at θ_B, to zero, at θ_1. A similar lower limiting angle, θ_2, occurs for which rays diffracted from adjacent planes have a phase difference of $\lambda - \delta\lambda$.

The magnitude of the angular range θ_1 to θ_2, and hence the breadth of the diffraction peak, is governed by the number of planes $2j$, and hence the crystal thickness. If the number of planes is very large, no significant broadening occurs because $\delta\lambda$ and therefore $(\theta_2 - \theta_1)$ is negligibly small. The commonly accepted formula for particle size broadening is the Scherrer formula:

$$t = \frac{0.9\lambda}{B\cos\theta_B} \tag{5.20}$$

where t is the thickness of the crystal (in angstroms), λ the X-ray wavelength and

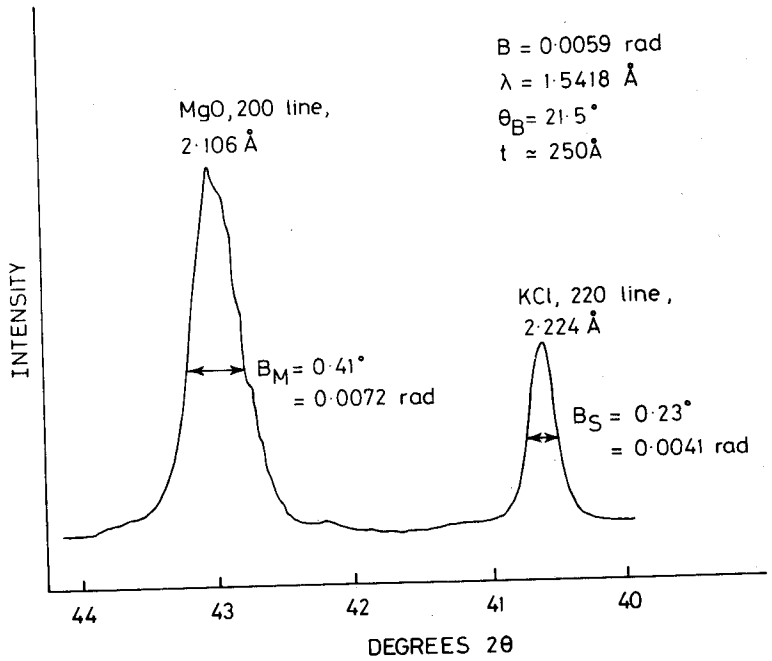

Fig. 5.45 Part of a diffractometer trace for a mixture of MgO (small particle size) and KCl (internal standard)

θ_B the Bragg angle. The line broadening, B, is measured from the extra peak width at half the peak height and is obtained from the Warren formula:

$$B^2 = B_M^2 - B_S^2 \tag{5.21}$$

where B_M is the measured peak width in radians at half peak height (Fig. 5.45) and B_S is the corresponding width of a peak of a standard material, mixed in with the sample, whose particle size is considerably greater than 2000 Å and which has a diffraction peak near to the relevant peak of the sample.

With good experimental techniques, broadening of high angle lines may be detected for crystal thickness up to ~ 2000 Å (e.g. for a crystal containing 2000 planes of d-spacing 1 Å). For a thickness of 50 to 500 Å the broadening is very easy to detect and measure (Fig. 5.45). The lower limit of detection occurs when the peaks become so broad that they disappear into the background radiation. For very small particle size, it is best to use low angle peaks if possible because, for a given crystal thickness, the broadening increases with angle. In extreme cases, peaks may be observable at low angles while high angle peaks cannot be distinguished from the background.

5.6.6 Effect of stress on a powder pattern

Crystals that are under stress may exhibit anomalous powder patterns. The whole powder pattern may be shifted to lower d-spacings if the crystals are under a uniform compressive stress such that a contraction of the unit cell occurs. If the stress is non-uniform, different crystals or different parts of the same crystal may be deformed to differing degrees and the powder lines become broadened. Commonly, both effects occur and lines may be both displaced and broadened.

Stresses may be (a) caused by the application of an external pressure or (b) generated internally as a consequence of a chemical reaction taking place inside the crystals. An example of (a) is the work hardening of metals in which residual distortions are present in the crystals after treatment. Examples of (b) are more varied and include coherent precipitation of supersaturated solid solutions (age hardening of metals and ceramics) and the occurrence of some phase transitions during cooling (if there is a change in volume or shape of the crystals and they are embedded in a solid matrix, then the rigid environment of the matrix may prevent the transition from occurring to completion).

5.6.7 Refinement of unit cell parameters and indexing of powder patterns

Unit cell parameters are often determined with the aid of single crystal X-ray photographs. The symmetry or unit cell type is first obtained from an inspection of the photographs. Positions of selected spots are then measured as accurately as possible to give values for the unit cell parameters. There are several intrinsic limitations to the accuracy of the values thus obtained—lack of internal standard, shrinkage of film, etc.—and accuracy of axial parameters is usually to between 0.05 and 0.2 per cent. Angles (for monoclinic and triclinic unit cells) can

usually be measured to about 1°*. For many materials and applications, such values are sufficiently accurate, e.g. if determination of the unit cell is merely one step in solving a crystal structure. It is very often the case, however, especially in solid state chemistry, that there is intrinsic interest in the powder patterns of crystalline phases and more accurate cell dimensions are desired. It is usually essential to assign Miller indices to the powder lines and often a line cannot be indexed unambiguously if the cell parameters are known only approximately. On the other hand, accurate cell parameters may be obtained from a least squares refinement on the d-spacings of at least several high angle powder lines whose indexing is known for certain. A circular situation may exist in which the determination of accurate lattice parameters and indexing of the powder pattern are intimately related and one is not possible without knowledge of the other. Usually, with patience, the problem can be solved by an iterative method especially if at least a few low angle lines may be indexed unambiguously. Least squares refinement of their d-spacings lead to more accurate cell parameters. The theoretical d-spacings calculated for these new cell parameters then enable a few more lines to be indexed with certainty and the least squares cycle is repeated. By this method, axial parameters may be obtained routinely accurate to 0.002 per cent and angles accurate to $\sim 0.1°$.

For powder patterns which are particularly difficult to index, i.e. for which there are two or more plausible sets of (hkl) values for some or all of the lines, single crystal photographs may be additionally useful. The intensities of the various candidate (hkl) reflections may be estimated qualitatively from the indexed single crystal photographs and the strongest of these almost certainly corresponds to the reflection that gives the powder line. This is because spots that are weak on single crystal photographs are not usually observed in powder photographs unless the latter are grossly overexposed.

Various computer programs are available with which one can supposedly index powder patterns without the necessity for prior knowledge of the crystal system. Great care must be exercised in using these programs since they can give information on the unit cell and cell parameters which may be incorrect or misleading. If one has an independent check that a particular unit cell, which has been used in the program to index the powder lines, is indeed the correct one, then these programs are useful; if not, the results are, at best, only tentative.

Problems may arise particularly for crystals which have neither cubic nor triclinic crystal systems. For cubic materials, the d-spacings are controlled by only one parameter, the cubic cell edge a, and it is a straight forward matter to index cubic powder patterns. For triclinic crystals, there is no single unit cell which is the correct one and the choice of unit cell is of no great consequence. For all other crystal systems, however, the powder patterns are controlled by two or more variables and computer fitting of d-spacing data with speculative unit cell parameters is not necessarily reliable.

*Greater accuracy is obtained using modern single crystal diffractometers, typically 0.03% for axes and ± 0.05° for angles.

5.6.8 Sources of background radiation—fluorescence

The quality of an X-ray powder diffraction pattern is governed to a considerable extent by the level of background radiation which is present. In mild cases it may be difficult to pick out the weaker reflections but in serious cases, as when *fluorescence* occurs, the intensity of all the diffracted beams may be reduced considerably at the same time that a large increase in background scattering occurs.

Several sources of background scattering, with their remedies, are as follows:

(a) Collisions between air molecules and diffracted X-ray beams. For high quality Guinier focusing films it is worth while to evacuate the box containing the sample and film.

(b) The presence of white radiation in the incident beam. This is best eliminated by using a single crystal monochromator.

(c) Fluorescence. This occurs when the sample acts as a secondary source of X-rays. If the fluorescent radiation is weak it may be absorbed by placing a filter between the sample and detector, e.g. a strip of nickel foil placed over the film. If it is strong, it is best to change the wavelength of the primary beam, e.g. by replacing an X-ray tube containing a copper target by one with an iron or molybdenum target.

Fluorescence occurs when the radiation in the primary beam (i.e. emitted by the copper target) knocks out inner shell electrons within atoms of the sample. Electrons in the outer shells drop down to occupy empty levels in the inner shells and, in so doing, they emit their excess energy in the form of X-rays. The sample is therefore acting as a secondary source of X-rays. The amount of fluorescent radiation produced in this way depends on the atomic number of the atoms in the sample relative to that of the target material and is best seen by example. Cu $K\alpha$ radiation, of wavelength 1.5418 Å, is generated by the electronic transition $2p \rightarrow 1s$ (Fig. 5.1). In order to create a vacant $1s$ level in the first place, the $1s \rightarrow \infty$ ionization potential is needed and this energy difference corresponds to a wavelength for copper of 1.3804 Å, Fig. 3.19. Incident X-rays of wavelength somewhat less than or equal to 1.3804 Å may therefore ionize a Cu/$1s$ electron. Similarly, Cu $K\alpha$ X-rays may ionize electrons in atoms whose ionization energy has a value corresponding to $\lambda > 1.5418$ Å. Ionization potentials of $1s$ electrons in nickel, cobalt and iron correspond to 1.4880, 1.6081 and 1.7433 Å and therefore Cu $K\alpha$ radiation may ionize $1s$ electrons in cobalt and iron but not in nickel. Samples containing cobalt and iron fluoresce strongly in Cu $K\alpha$ radiation. Lighter atoms also fluoresce, but less strongly, since fluorescence is strongest when the incident radiation has a wavelength that is only slightly shorter than the absorption edge ($\equiv IP$) of the atoms.

(d) Compton scattering. When an X-ray beam strikes a sample two types of scattered X-rays are produced. In the first, the incident beam sets the electrons of the atoms in to vibration; X-rays of the same wavelength as the incident beam are re-emitted and are the characteristic diffracted radiation

with which we are familiar. This is called *coherent, unmodified radiation.* The incident X-ray beam may also interact inelastically with the outer, more loosely bound electrons of the sample atoms. Some of the energy of the X-rays is inevitably lost and the resulting scattered X-rays, *modified Compton X-rays,* have slightly longer wavelength than the incident beam. Compton scattering contributes to the general background scatter and is particularly serious for the lighter elements. For this reason, organic and organic-based (e.g. polymeric) materials may give poor quality powder patterns, due to the combined effects of reduced diffracted intensity and increased background intensity. The intensity of Compton scattering increases with increasing angle (in contrast to diffracted radiation which decreases in intensity at higher angles; see Section 5.5) and so it is common to see powder patterns of, for example, polymers which have well-defined strong lines at high d-spacings but only a general background scattering at lower d-spacings. There is no real remedy for Compton scattering.

(e) Crystal imperfections and temperature diffuse scattering. Any kind of imperfection in the crystals of the sample causes a certain amount of diffuse scattering at angles other than the various Bragg angles. It cannot be avoided. The ideal powder pattern is obtained for crystals with perfect three-dimensional regularity, free from strain, imperfections, surface effects and at absolute zero. The effect of small particle size and non-uniform stress on powder peaks has been mentioned earlier. Atomic vibrations are an important source of diffuse scattering and these increase as the melting point is approached. It is particularly noticeable in high temperature powder diffraction results that the intensities of powder lines get progressively weaker as the temperature is raised and at the same time the background scattering increases. A useful guideline is that for a given material and set of conditions the total diffracted intensity is constant. If peak intensities are reduced, the intensity must reappear elsewhere—probably in the background.

5.6.9 A powder pattern is a crystal's 'fingerprint'

The powder X-ray diffraction method is very important and useful in qualitative phase analysis because every crystalline material has its own characteristic powder pattern; indeed, the method is often called the powder fingerprint method. There are two main factors which determine powder patterns: (a) the size and shape of the unit cell and (b) the atomic number and position of the various atoms in the cell. Thus, two materials may have the same crystal structure but almost certainly they have quite distinct powder patterns. For example, KF, KCl and KI all have the rock salt structure and should show the same set of lines in their powder patterns, but, as can be seen from Table 5.7, both the positions and intensities of the lines are different in each. The positions or d-spacings of the lines are shifted because the unit cells are of different size and, therefore, the a parameter in the d-spacing formula varies. Intensities are different

because different anions with different atomic numbers and therefore different scattering powers are present in the three materials, even though the atomic coordinates are the same for each (i.e. cations at corner and face centre positions, etc.). KCl is a rather extreme example because the intensities of 111 and 311 reflections are too small to measure, but it serves to illustrate the importance of scattering power of the atoms present. Intensities are discussed in more detail in Section 5.5.

The powder pattern has two characteristic features, therefore: the d-spacings of the lines and their intensity. Of the two, the d-spacing is far more useful and capable of precise measurement. The d-spacings should be reproducible from sample to sample unless impurities are present to form a solid solution or the material is in some stressed, disordered or metastable condition. On the other hand, intensities are more difficult to measure quantitatively and often vary from sample to sample. Intensities can usually be measured only semi-quantitatively and may show variation of, say, 20 per cent from sample to sample (much more if preferred crystal orientation is present). Thus, the differences in tabulated intensities for, say, the 220 reflection of the three materials in Table 5.7 are probably not too significant.

The likelihood of two materials having the same cell parameters and d-spacings decreases considerably with decreasing crystal symmetry. Thus, cubic materials have only one variable, a, and there is a fair chance of finding two materials with the same a value. On the other hand, triclinic powder patterns have six variables, a, b, c, α, β and γ, and so accidental coincidences are far less likely. Problems of identification, if they occur at all, are most likely to be experienced with high symmetry, especially cubic, materials.

5.6.10 Structure determination from powder patterns

Although structure determination is normally carried out using single crystal X-ray data, there are instances where powder data can be used and may even be advantageous. The structures of metals and alloys have generally been solved from powder data. They are often cubic, hexagonal or tetragonal and it is a straightforward exercise to index their powder patterns and calculate the cell dimensions. Many or all of the atoms in the unit cell lie on special positions such as the origin, face centres, body centres, etc., and so the number of positional parameters which is variable and must be determined is either small or zero. The proposed structure can then be confirmed by comparing the intensities calculated from the model with those observed experimentally; there may be only 5 to 10 lines observed in the powder pattern but this is sufficient for the purpose.

Structure determination of non-metallic materials by the powder method is rather more difficult because these materials often have unit cells of low symmetry and/or there are a considerable number of positional variables for the atoms in the unit cell. Occasionally, if a suitable single crystal of the new phase cannot be obtained and if the crystal system and unit cell parameters may be determined

by electron diffraction, the powder intensities may be used for a structure determination (electron diffraction intensities are very unreliable, even when compared with powder X-ray intensities). The limit to the complexity of structure which can be tested is governed by the number of powder lines whose intensities can be measured and whose indexing is known for certain. Solving a structure is akin to solving a set of simultaneous equations; there must not be more variables than equations if the equations are to be solved.

Although the powder method is not often used for the determination of completely unknown structures it does have many secondary uses related to crystal structures and can be a relatively quick method of obtaining results. For example, suppose that one has prepared a new phase which apparently has a perovskite structure. Computer programs are available which generate a calculated powder pattern from a given set of atomic coordinates. Into the program are fed the coordinates of the proposed structure together with the scattering factor data for the atoms in the structure. The program then calculates the intensities of all possible reflections and these may be compared with the observed powder intensities of the new phase in order to judge whether or not the postulated structure is correct.

In the above example, no refinement in atomic coordinates of a proposed structure is carried out; all that is done is to test a proposed model for correctness. Other cases exist where a limited part of a structure may be in doubt and powder data may be used to decide which of the various possibilities is correct. Good examples are spinels. These may be normal, inverse or intermediate; the different forms are distinguished by the way in which some or all of the cations arrange themselves over the available sites. For a particular material the powder pattern may be calculated for different cation arrangements and that which gives best agreement between observed and calculated intensities is probably correct. For problems such as this there is really no need for single crystal data and solution of the problem can be obtained within a matter of days instead of the weeks or months that are needed to carry out a single crystal analysis.

It has already been mentioned that powder data may be used for the study of materials which cannot be prepared in suitable-sized single crystal form. A related use is in the crystallographic study of materials at high temperatures. High temperature single crystal methods are not often used whereas high temperature powder diffractometry is an established technique. The structural transition at $\sim 270\,^{\circ}C$ in cristobalite, SiO_2, has been followed by powder diffractometry. The structure of the high temperature form was solved—it has a disordered structure with a choice of six positions for each oxygen in a non-linear Si–O–Si bridge—and the changes that occur during the low–high transition were deduced.

Powder X-ray methods are invaluable for obtaining structural information about solid solutions—substitutional, interstitial or otherwise—and order–disorder phenomena in, for example, alloys. A further discussion is given in Chapter 10.

5.6.11 Powder patterns from single crystals—the Gandolfi camera

There are several instances where it may be desirable to have the powder pattern appropriate to a single crystal sample. To achieve this, a modified Debye–Scherrer camera, known as the Gandolfi camera, is used. In this camera, the crystal sample is stuck onto a fibre and mounted on a rotation device. This device causes the crystal to rotate, simultaneously and at different angular velocities, about two axes. Over a period of time, the crystal presents itself to the X-ray beam in a very large number of orientations. A completely random time-averaged orientation of the crystal is not achieved but nevertheless a sufficiently large number of orientations is presented that a recognizable powder pattern may be obtained after an exposure time of 1 to 2 days.

The Gandolfi camera is used in mineralogy in cases where a specimen is rare or unusual and should be preserved intact rather than crushed up in order to take a conventional X-ray powder pattern. In other cases only one or two grains of a particular crystalline phase may be available and there is insufficient material for a conventional powder pattern.

5.6.12 Powder patterns calculated from crystal structure data

Crystal structures are solved using intensity data, usually from single crystals but occasionally from powders (Section 5.6.10). It is sometimes useful to carry out the reverse exercise and, for a known crystal structure, calculate the corresponding powder pattern. This involves calculation of the d-spacings at which lines appear and their corresponding intensities. Calculation of d-spacings is straightforward and requires knowledge only of the unit cell dimensions and the appropriate d-spacing formula (see Section 5.3.7 and Appendix 6). Calculation of intensities is a little more complicated and requires a knowledge of the crystal structure and, in particular, the coordinates of all the atoms in the unit cell. The first step is to calculate the structure factors, F_{hkl}^{calc}, for all possible reflections of interest. The procedure for doing this is given in Section 5.5.3. The second step is to convert the structure factors to intensities (equation 5.18) and correct for the L_p factors and multiplicities.

Calculated powder patterns have several uses. They can be used:

(a) to provide reference intensity data for materials which are subject to preferred orientation, e.g. crystals with a platy texture,
(b) to show that a single crystal, whose structure has been solved, is representative of a bulk sample from which the crystal was taken,
(c) if observed and calculated powder patterns match well, to confirm that a new crystalline phase has the crystal structure which has been postulated for it,
(d) to generate powder patterns for hypothetical crystal structures and
(e) to assist in indexing complex powder patterns, i.e. in deciding the appropriate *hkl* values for a particular powder line.

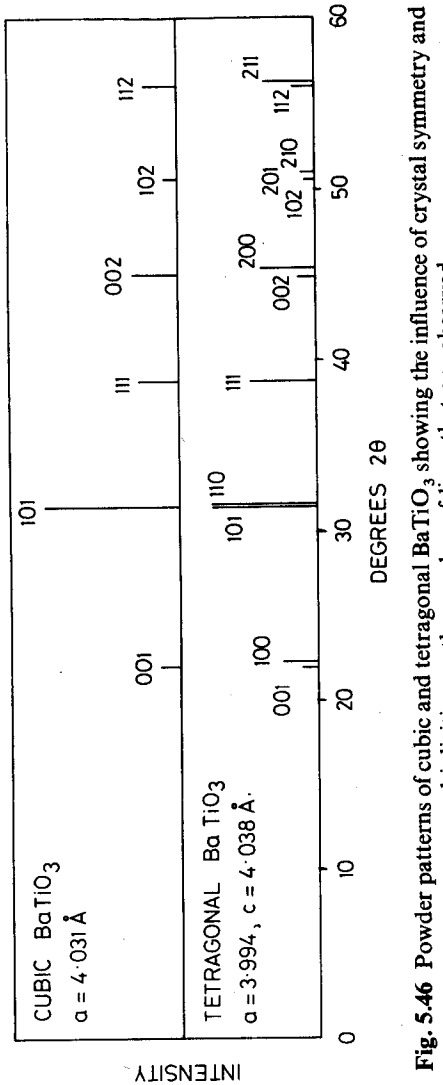

Fig. 5.46 Powder patterns of cubic and tetragonal $BaTiO_3$ showing the influence of crystal symmetry and multiplicities on the number of lines that are observed.

5.6.13 Influence of crystal symmetry and multiplicities on powder patterns

A general observation about the relative complexity of powder patterns is that the number of lines which appear increases with decreasing crystal symmetry. Thus, simple cubic substances give only a few lines whereas triclinic materials may give up to a hundred. This is explained in Section 5.3.10 as being due to the effect of multiplicity; cubic materials do have a large number of lines, just as many as a material with a similar sized, triclinic unit cell, but in cubic materials, many of the lines overlap and the number of distinct lines that may be seen is greatly reduced. A simple example of this is shown in Fig. 5.46; schematic powder patterns are given for two polymorphs of the perovskite phase, $BaTiO_3$. One polymorph is cubic. The other is tetragonal but the distortion from a cubic-shaped unit cell is not large; the *c* axis is about 1 per cent longer than *a*. As can be seen in Fig. 5.46, the tetragonal distortion leads to an increase in the number of observed powder lines. Thus 001 and 100 appear as separate lines because they have different *d*-spacings, whereas they overlap in the cubic polymorph; similarly 110 and 101 ($\equiv$ 011) appear as separate lines in the tetragonal polymorph but overlap in the cubic form. Not all lines in the cubic form separate into doublets in

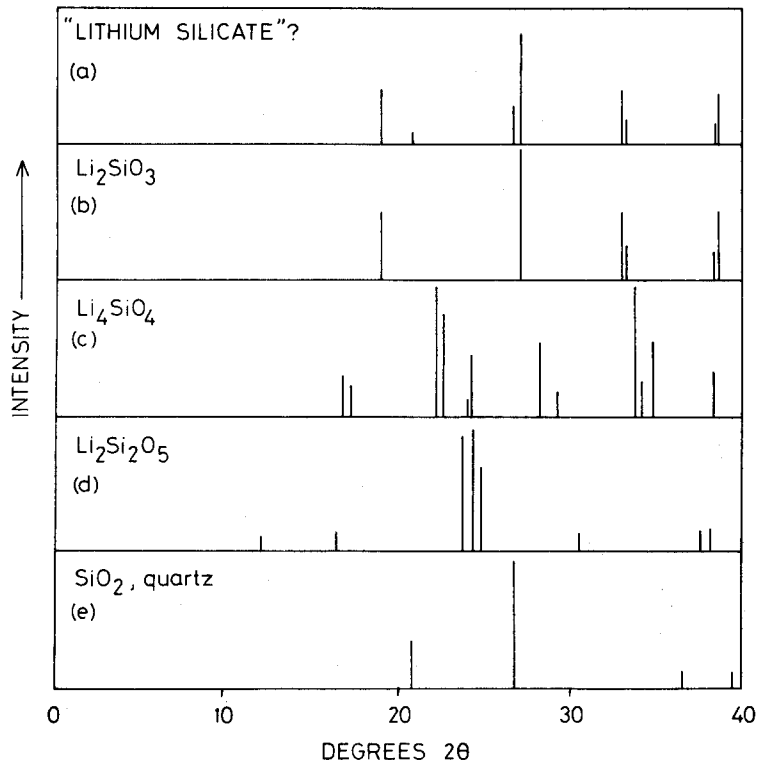

Fig. 5.47 Powder patterns of (a) a bottle labelled 'lithium silicate' and (b) to (e) standard lithium silicate and silica phases

the tetragonal form, however. Thus, 111 stays as a single line but 102 separates into three lines, 102, 201 and 210.

5.6.14 Powder patterns of mixtures of phases

Mixtures of crystalline phases may be analysed very easily and effectively using Guinier films. An illustration of the method is given in Fig. 5.47. Some time ago, the author purchased a bottle of what was advertised as Li_4SiO_4. The bottle arrived labelled 'lithium silicate'; part of its X-ray powder pattern is shown schematically in (a) together with patterns of standard lithium silicate phases and silica in (b) to (e). Comparison of the films showed that the bottle contained predominantly Li_2SiO_3 and a small amount of quartz, but none of the expected phase, Li_4SiO_4!

Questions

5.1 Using the $K\alpha_1$ data of Table 5.1, verify graphically Moseley's Law. What wavelength do you expect for Co $K\alpha_1$ radiation?

5.2 What symmetry elements do the following tetrahedral-shaped molecules possess: (a) CH_3Cl, (b) CH_2Cl_2, (c) CH_2ClBr?

5.3 Show that the following Bravais lattices are equivalent:
(a) C-tetragonal and P-tetragonal
(b) F-tetragonal and I-tetragonal
(c) B-monoclinic and P-monoclinic (b unique axis)
(d) C-monoclinic and I-monoclinic (b unique axis)

5.4 What is the probable lattice type of crystalline substances that give the following observed reflections?
(a) 110, 200, 103, 202, 211
(b) 111, 200, 113, 220, 222
(c) 100, 110, 111, 200, 210
(d) 001, 110, 200, 111, 201

5.5 Calculate the 2θ and d values for the first five lines in the X-ray powder pattern, Cu $K\alpha$ radiation, of a primitive cubic substance with $a = 5.0$ Å. What is the multiplicity of each line?

5.6 At 20 °C, Fe is body centred cubic, $Z = 2$, $a = 2.866$ Å. At 950 °C, Fe is face centred cubic, $Z = 4$, $a = 3.656$ Å. At 1425 °C, Fe is again body centred cubic, $Z = 2$, $a = 2.940$ Å. At each temperature, calculate (a) the density of iron, (b) the metallic radius of iron atoms.

5.7 The value of n in Bragg's Law is always set equal to 1. What happens to the higher order diffraction peaks?

5.8 Silver oxide, Ag_2O, has a cubic unit cell, $Z = 2$, with atomic coordinates Ag: $\frac{1}{4}\frac{1}{4}\frac{1}{4}$, $\frac{3}{4}\frac{3}{4}\frac{1}{4}$, $\frac{3}{4}\frac{1}{4}\frac{3}{4}$, $\frac{1}{4}\frac{3}{4}\frac{3}{4}$; O: 000, $\frac{1}{2}\frac{1}{2}\frac{1}{2}$. What are the atomic coordinates if the unit cell is displaced so that an Ag atom is at the origin? What is the lattice type of Ag_2O? What is the coordination number of Ag and O? Does the structure possess a centre of symmetry?

5.9 A cubic alkali halide has its first six lines with d-spacing 4.08, 3.53, 2.50, 2.13, 2.04 and 1.77 Å. Assign Miller indices to the lines and calculate the value of the unit cell dimension. The alkali halide has density 3.126 g cm^{-3}. Identify the alkali halide.

5.10 An imaginary orthorhombic crystal has two atoms of the same kind per unit cell located at 000 and $\frac{1}{2}\frac{1}{2}0$. Derive a simplified structure factor equation for this. Hence, show that, for a C-centred lattice, the condition for reflection is hkl: $h + k = 2n$.

5.11 Derive a simplified structure factor master equation for the perovskite structure of $SrTiO_3$. Atomic coordinates are Sr: $\frac{1}{2}\frac{1}{2}\frac{1}{2}$; Ti: 000; O: $\frac{1}{2}00$, $0\frac{1}{2}0$, $00\frac{1}{2}$.

5.12 The 111 reflection in the powder pattern of KCl has zero intensity but in the powder pattern of KF it is fairly strong. Explain.

5.13 The alloy gold–copper has a face centred cubic unit cell at high temperatures in which the Au, Cu atoms are distributed at random over the available corner and face centre sites. At lower temperatures, ordering occurs: Cu atoms are located preferentially on the corner sites and one pair of face centre sites; Au atoms are located on the other two pairs of face centre sites. What effects would you expect this ordering process to have on the X-ray powder pattern?

5.14 The X-ray powder pattern of orthorhombic Li_2PdO_2 includes the following lines: 4.68 Å (002), 3.47 Å (101), 2.084 Å (112). Calculate the values of the unit cell parameters. The density is 4.87 g cm^{-3}; what are the cell contents?

5.15 An ammonium halide, NH_4X, has the CsCl structure at room temperature, $a = 4.059$ Å, and transforms to the NaCl structure at 138 °C, $a = 6.867$ Å.
(a) The density of the room temperature polymorph is 2.431 g cm^{-3}. Identify the substance.
(b) Calculate the d-spacings of the first four lines in the powder pattern of each polymorph.
(c) Calculate the percentage difference in molar volume between the two polymorphs, ignoring thermal expansion effects.
(d) Assuming an effective radius of 1.50 Å for the spherical NH_4^+ ion and that anions and cations are in contact, calculate the radius of the anion in each structure. Are the anions in contact in the two structures?

5.16 'Each crystalline solid gives a characteristic X-ray powder diffraction pattern which may be used as a fingerprint for its identification.' Discuss the reasons for the validity of this statement and indicate why two solids with similar structures, e.g. NaCl and NaF, may be distinguished by their powder patterns.

5.17 Show by means of qualitative sketches the essential differences between the X-ray powder diffraction patterns of (a) a 1:1 mechanical mixture of powders of NaCl and AgCl and (b) a sample of (a) that has been heated to produce a homogeneous solid solution.

5.18 A sample of aluminium hydroxide was shown by chemical analysis to contain a few per cent of Fe^{3+} ions as impurity. What effect, if any, would